



HAL
open science

Nanocomposite sponges for enhancing intestinal residence time following oral administration

Annalisa Rosso, Valentina Andretto, Yves Chevalier, David Kryza, Jacqueline Sidi-Boumedine, Ana Grenha, Filipa Guerreiro, Adem Gharsallaoui, Veronica La Padula, Alexandra Montembault, et al.

► To cite this version:

Annalisa Rosso, Valentina Andretto, Yves Chevalier, David Kryza, Jacqueline Sidi-Boumedine, et al.. Nanocomposite sponges for enhancing intestinal residence time following oral administration. *Journal of Controlled Release*, 2021, 10.1016/j.jconrel.2021.04.004 . hal-03202389

HAL Id: hal-03202389

<https://hal.science/hal-03202389>

Submitted on 24 Apr 2023

HAL is a multi-disciplinary open access archive for the deposit and dissemination of scientific research documents, whether they are published or not. The documents may come from teaching and research institutions in France or abroad, or from public or private research centers.

L'archive ouverte pluridisciplinaire **HAL**, est destinée au dépôt et à la diffusion de documents scientifiques de niveau recherche, publiés ou non, émanant des établissements d'enseignement et de recherche français ou étrangers, des laboratoires publics ou privés.



Distributed under a Creative Commons Attribution - NonCommercial 4.0 International License

1 Nanocomposite sponges for enhancing intestinal residence time following oral administration

2

3 Annalisa Rosso¹, Valentina Andretto¹, Yves Chevalier¹, David Kryza^{1,2}, Jacqueline Sidi-Boumedine¹,
4 Ana Grenha³, Filipa Guerreiro³, Adem Gharsallaoui¹, Veronica La Padula⁴, Alexandra Montembault⁵,
5 Laurent David⁵, Stéphanie Briçon¹ and Giovanna Lollo¹

6

7 1. Univ Lyon, Université Claude Bernard Lyon 1, CNRS, LAGEPP UMR 5007, 43 Boulevard du 11
8 Novembre 1918, F-69622, Villeurbanne, France

9 2. Hospices Civils de Lyon, 69437 Lyon, France

10 3. Centre for Marine Sciences (CCMAR), Universidade do Algarve, Campus de Gambelas, 8005-139
11 Faro, Portugal

12 4. Centre Technologique des Microstructures (CTμ), Université Claude Bernard Lyon 1, France

13 5. Univ Lyon, Université Claude Bernard Lyon 1, CNRS, Ingénierie des Matériaux Polymères (IMP)
14 UMR 5223, 15 boulevard Latarjet, F-69622, Villeurbanne, France

15

16 Corresponding author email: giovanna.lollo@univ-lyon1.fr

17

18

19 Abstract

20 In this work, nanocomposites that combine mucopenetrating and mucoadhesive properties in a single
21 system are proposed as innovative strategy to increase drug residence time in the intestine following
22 oral administration. To this aim, novel mucoadhesive chitosan (CH) sponges loaded with
23 mucopenetrating nanoemulsions (NE) were developed via freeze-casting technique. The NE
24 mucopenetration ability was determined studying the surface affinity and thermodynamic binding of the
25 nanosystem with mucins. The ability of nanoparticles to penetrate across a preformed mucins layer
26 was validated by 3D-time laps **Confocal Laser Scanning Microscopy** imaging. Microscopy observation
27 (Scanning Electron Microscopy and Optical Microscopy) showed that NE participated in the structure
28 of the sponge affecting its stability and the *in vitro* release kinetics of NE. **When incubated with HCT**
29 **116 and Caco-2 cell lines, the NE proved to be cytocompatible over a wide concentration range.**
30 Finally, the *in vivo* biodistribution of the nanocomposite was evaluated after oral gavage in healthy
31 mice. The intestinal retention of NE was highly enhanced when loaded in the sponge compared to the
32 NE suspension. Overall, our results demonstrated that the developed nanocomposite sponge is a
33 promising system for sustained drug intestinal delivery.

34

35 Keywords

36 Nanocomposite, nanoemulsion, chitosan sponge, oral administration, intestinal drug delivery.

37

38

39 Introduction

40 The development of drug delivery strategies able to control and sustain drug release after oral
41 administration can be achieved using systems that are biocompatible, mechanically flexible, and
42 steady over time [1–3]. Upon oral administration, drugs face acidic environment and enzymatic
43 degradation in the stomach, which limit their availability. Once in the intestine, further obstacles are the
44 presence of the intestinal mucus gel layer that hinders drug delivery to the underlying epithelium, and
45 the mucus turnover that enhances drug excretion [4]. To overcome these biological hurdles and

1 increase the residence time of active compounds in the gastro-intestinal (GI) tract, mucoadhesive and
2 mucopenetrating drug delivery nanosystems have been extensively explored [5,6]. Mucoadhesive
3 nanosystems coated with bioadhesive polymers (chitosans, alginates, and acrylic derivatives) are able
4 to interact with the mucus layer through electrostatic, H-bonding and/or hydrophobic interactions [1,7–
5 9]. This strategy allows the particle to remain intimately attached to the mucins gel, however
6 premature cargo release and/or accumulation inside the mucosal layer could occur [10]. On the
7 contrary, mucopenetrating nanocarriers can spread over the mucosa, penetrate deep mucus regions
8 and reach the intestinal epithelium [11,12]. A reduction of interactions with mucins is provided by a
9 neutral surface charge of the particles, resulting from the coating with non-ionic polymers such as
10 poly(ethylene glycol) (PEG) [13–15]. An improvement strategy consists in the development of
11 nanocomposites made of mucopenetrating nanoparticles integrated into biocompatible mucoadhesive
12 macrostructures. Thereby, nanosystems can be released from the composite in a controlled and “on-
13 demand” fashion, assisting site-specific drug targeting, and finally interact with the epithelial surface
14 [6]. For the development of such mucoadhesive macrosystems, hydrogels based on polysaccharides
15 have been extensively studied [3,16–19]. However, because of their semi-solid properties and
16 hydrated nature, hydrogels presented practical concerns such as the limited stability during storage
17 and the dependence of the hydrogel network properties on the physiological conditions (pH,
18 enzymes). This can shorten the *in vivo* residence time or trigger burst drug release [17,20]. To address
19 this issue, dry porous 3D systems such as sponges have been designed. Sponges are obtained via
20 the controlled solidification of polymers and colloidal suspensions by mean of freeze-casting technique
21 [21–23]. Sponges can improve mucoadhesion thanks to their porous structure, while providing a
22 sustained drug release [24,25]. The dry state guarantees a high system stability for storage and offers
23 an *in situ* activable platform upon hydration in biological fluids [26]. The incorporation of drug delivery
24 systems inside sponges’ macro- or microstructures can also refine the intestinal targeting ability [27].
25 Nanocomposites have been proved to enhance the systemic absorption [2,28] or to maximize the local
26 effect of drugs [3]. Their exploitation is currently under investigation for the treatment of different
27 pathological conditions including obesity, diabetes, colon cancer and inflammatory disorders, such as
28 ulcerative colitis and Crohn’s disease [3,20,29,30].

29 We recently developed novel nanoemulsions (NE), composed of an oil core surrounded by a non-ionic
30 PEGylated surfactant shell, which hold promising features as a mucopenetrating drug delivery system
31 [31]. In this work, we aimed at developing chitosan (CH) sponges loaded with NE as nanocomposites
32 to control and prolong drug intestinal delivery. To reach this objective our strategy was focused on
33 increasing the intestinal residence time of such nanocomposite via the combination of
34 mucopenetrating (NE) and mucoadhesive (CH sponge) properties in a single delivery system.

35 Chitosan is a high mucoadhesive polysaccharide regarded as non-toxic, biocompatible and
36 biodegradable. Its adhesion capacity to the mucosal epithelium has been largely described and arises
37 mainly from the electrostatic binding with anionic glycoproteins of mucins in the intestine [32,33]. In
38 particular, the low pH of inflamed zones can favour such interactions increasing its mucoadhesive
39 ability [18]. We hypothesized that the CH sponge can prolong the drug retention time in the intestine
40 by adhering to the mucus and allow a controlled release of the embedded NE. To validate our
41 approach, we firstly assessed the mucopenetrating ability of NE. Then, NE-loaded CH sponges (CH-
42 NE) obtained by freeze-casting technique, were characterized regarding their structural and
43 mechanical properties. The impact of the CH sponge on NE release kinetics was investigated after
44 sponge re-hydration in simulated intestinal fluids. The cytocompatibility of the system was assessed
45 on human colorectal carcinoma cells (HCT 116 and Caco-2). Finally, *in vivo* biodistribution studies of

1 both fluorescent NE and CH-NE after oral gavage to mice were performed to assess the ability of the
2 nanocomposite to increase the residence time of NE in the intestine.

4 **2. Material and methods**

5 **2.1. Materials**

6 Medium chain triglycerides, MCT (Miglyol®812), was purchased from Cremer Oleo GmbH & Co. KG
7 (Hamburg, Germany). Polyoxyethylene (40) stearate (Myrj®52), Nile red (NR), curcumin (CCM), formic
8 acid, sodium dodecyl sulphate (SDS), mucin from porcine stomach Type II and Dulbecco's modified
9 Eagle's medium (DMEM) were purchased from Sigma-Aldrich (St Quentin-Fallavier, France). Oleoyl
10 polyoxyl-6 glycerides (Labrafil®M1944CS) was provided by Gattefossé (Saint-Priest, France). Egg
11 phospholipids with 70% phosphatidylcholine (Lipoid®E80S) were obtained from Lipoid GmbH
12 (Ludwigshafen am Rhein, Germany). Potassium dihydrogen phosphate (KH₂PO₄) and potassium
13 chloride (KCl) were purchased from Riedel-de-Haën AG (Seelze, Germany). Di-sodium hydrogen
14 orthophosphate dihydrate (Na₂HPO₄·2H₂O) was purchased from Serva Electrophoresis GmbH
15 (Heidelberg, Germany). Sodium chloride (NaCl), hydrochloric acid (HCl) 37%, phosphate buffered
16 saline (PBS) tablets (pH 7.4), 3-(4,5-dimethylthiazol-2-yl)-2,5-diphenyltetrazolium (MTT) were obtained
17 from VWR International (Fontenay-sous-Bois, France). Penicillin/streptomycin (10000 U·mL⁻¹), foetal
18 bovine serum (FBS) and nanomycopulitine from Dutscher SAS (Brumath, France). Acetic acid was
19 obtained from Chem-Lab NV (Zedelgem, Belgium). Dichloromethane, methanol, ethanol, acetonitrile
20 (HPLC grade), sodium taurocholate hydrate 96%, sodium hydroxide (NaOH), DiC₁₈(5) solid, 1,1'-
21 dioctadecyl-3,3,3',3'-tetramethylindodicarbocyanine, 4-chlorobenzene sulfonate salt
22 (DiD) and Promega CellTiter 96™ AQueous One Solution Cell Proliferation Assay (3-(4,5-
23 dimethylthiazol-2-yl)-5-(3-carboxymethoxyphenyl)-2-(4-sulfophenyl)-2H-tetrazolium), MTS were
24 purchased from Thermo Fisher Scientific (Illkirch, France). Milli-Q® water was obtained using a Milli-
25 Q® Academic System from Merck-Millipore (Saint-Quentin-en-Yvelines, France). The aqueous phase
26 used to prepare NE was phosphate buffer saline solution (PBS 5 mM, pH 7.4). The aqueous phase
27 used to prepare mucin gels was Sorenson's phosphate buffer containing Na₂HPO₄ and KH₂PO₄
28 (0.2 M, pH 7.4).

29 The chitosan used in this study was produced from N-deacetylation of chitin extracted from squid pens
30 and was purchased from Mahtani Chitosan (batch type 114). Its structural properties are the following:
31 a degree of acetylation of 4.0 ± 0.5%, a weight-average molar mass M_w of 550 ± 50 kg·mol⁻¹ and a
32 dispersity Đ of 1.5 ± 0.3. ¹H NMR analysis was used to determine the degree of acetylation (DA) of
33 chitosan [34]. M_w and Đ were determined as previously described [35], using size exclusion
34 chromatography (SEC) coupled online with a differential refractometer (Optilab T-rEX, Wyatt; λ=658
35 nm) and with a multi-angle laser light scattering (SEC-MALLS) detector (Dawn-HELOES II, Wyatt;
36 λ=664 nm).

38 **2.2. Process of nanoemulsions formulation**

39 NE were prepared by emulsion phase inversion (EPI) technique coupled with high stirring energy input
40 as previously described [31]. Briefly, NE were composed of an MCT oil core stabilized by a surfactant
41 shell, made of a mixture of hydrophilic and hydrophobic surfactants, namely polyoxyethylene (40)
42 stearate (Myrj®52) and oleoyl polyoxyl-6 glycerides (Labrafil®M1944CS), respectively. To prepare the
43 oil phase, MCT (0.35 g) and surfactants (1 g) were mixed and magnetically stirred (750 rpm) using a
44 thermostated bath at 80 °C. The aqueous phase (PBS 5 mM, 3.65 mL), heated up to 80 °C as well,
45 was added into the organic melt phase. Stirring was then performed by two cycles of 10 min using a

1 rotor-stator disperser (T25 digital Ultra-Turrax® equipped with a S25N-10G shaft, IKA®-Werke GmbH
2 & Co. KG, Staufen, Germany) rotating at 11000 rpm at 80 °C.

3 The hydrophobic dyes Nile red (NR), curcumin (CCM) and DiD were added to the oil phase during NE
4 preparation for their encapsulation in NE droplets. The final fluorescent probe concentrations in the NE
5 were NR 200 µg·mL⁻¹, CCM 500 µg·mL⁻¹, DiD 50 µg·mL⁻¹. NR or CCM were solubilized in the oil
6 phase and magnetically stirred (750 rpm) for 2 h at 80 °C to obtain a homogeneous mixture. NE were
7 then formulated as explained above. Regarding the lipophilic carbocyanine dye DiD, 125 µL of its
8 stock solution in ethanol (2 mg·mL⁻¹) were mixed with the oil phase and the NE were formulated
9 keeping the temperature below the DiD melting point (68 °C) in order to avoid dye decomposition.

11 2.3. Physico-chemical characterization of nanoemulsions

12 The size distribution and surface potential of the NE droplets were determined using Malvern
13 Zetasizer® Nano ZS instrument (Malvern Instruments S.A., Worcestershire, UK). The particle sizes
14 were measured by Dynamic Light Scattering (DLS) at 25 °C at a scattering angle of 173 °. The ζ-
15 potential was calculated from the mean electrophoretic mobility measured for samples diluted in 1 mM
16 KCl.

17 The stability of blank and CCM-NE in colloidal suspension was followed during 28 days upon storage
18 at 20 °C. At scheduled time points, particle size, polydispersity index (PDI) and ζ-potential were
19 measured. Moreover, dye leakage (CCM and NR) from NE was assessed at day 28. Free dye was
20 separated from the suspending aqueous medium by size exclusion chromatography on PD-10
21 Desalting Columns containing 8.3 mL of Sephadex™ G-25 resin (GE Healthcare Bio-Sciences AB,
22 Uppsala, Sweden). The NE containing fractions were easily identified thanks to their turbidity and
23 collected in microtubes.

24 For NR-loaded NE, 200 mg of isolated NE were dissolved in ethanol (1 g) and analysed by UV-vis
25 absorbance at 549 nm. The CCM-loaded NE fraction was analysed by HPLC equipped with an UV-vis
26 detector based on previously reported methods [36,37]. In order to quantify CCM, 300 mg of isolated
27 NE were dissolved in methanol (1 g) and the samples were vortexed for 5 min. The samples were
28 filtered using Nylon filter 0.22 µm (Whatman GmbH, Dassel, Germany) before injection in the HPLC
29 system. The HPLC apparatus consisted of Agilent 1200 Series G1311A Quat Pump, Agilent 1200
30 Series G1367B HIP-ALS High Performance Autosampler, equipped with Agilent 1200 Series G1315D
31 Dad Diode Array Detector HPLC (Agilent, Santa Clara, CA, United States). CCM was detected using a
32 RP-C18 column (Kinetex 5 µm C18 100 Å, 150 × 4.6 mm, Phenomenex, Torrance, CA, USA), set at
33 30 °C, using acetonitrile and deionized water 0.1% formic acid (50:50) as mobile phase at a flow rate
34 of 1.0 mL·min⁻¹. The injection volume was 10 µL, the detection wavelength 423 nm and the total run
35 time 8 min. The chromatogram of CCM exhibited a characteristic peak at a retention time 6.6 min.
36 Peak areas were recorded and processed on the OpenLab CDS ChemStation Edition software
37 (Agilent, Santa Clara, CA, United States). The HPLC calibration curve was linear (R² = 0.99) in the
38 concentration range of 0.04–40 µg·mL⁻¹. The method was validated according to ICH Q2(R1)
39 guidelines. Detection and quantification limits (LOD and LOQ) were 2.17 µg·mL⁻¹ and 7.24 µg·mL⁻¹,
40 respectively.

41 The encapsulation efficiency was calculated as the ratio of dye detected in the isolated NE (NE
42 purified: NE_p) to the amount of dye initially loaded in the NE (NE initial: NE_i):

$$43 \text{ Encapsulation efficiency (\%)} = \frac{NE_p}{NE_i} \times 100 \quad \text{Eq. 1}$$

44 All studies and measurements presented in this work were performed in triplicate.

1
2
3
4
5
6
7
8
9
10
11
12
13
14
15
16
17
18
19
20
21
22
23
24
25
26
27
28
29
30
31
32
33
34
35
36
37
38
39
40
41
42
43
44

2.4. Mucins-nanoemulsions interaction

2.4.1. Colloidal stability of nanoemulsions in mucins

Mucin solution from porcine stomach Type II (1% w/v) was prepared by suspending 40 mg of mucin powder in 4 mL of Sorenson's phosphate buffer (pH 7.4). The solution was magnetically stirred (750 rpm) for 2 h in an ice bath and left for equilibration overnight at 4 °C. Then, mucin solution and blank NE were mixed to obtain a final mucin concentration of 0.5% w/v and NE concentration of 0.5% w/v. Samples were magnetically stirred at 300 rpm for 4 h in a water bath at 37 °C. At predetermined time points (0.5, 1, 2, 3, and 4 h) an aliquot (1 mL) was retrieved and centrifuged at 7000 rpm for 5 min to separate mucin and entrapped NE from the supernatant. Then, the supernatant was collected and NE size distribution and ζ -potential were measured at 37 °C. The ζ -potential of NE (0.1% w/v) and mucin solutions (0.1% w/v) in PBS 5 mM was separately analysed at pH values ranging from 2 to 9. The pH was varied by titration of NaOH (0.1 M) or HCl (0.1 M).

2.4.2. Microcalorimetric studies

The thermodynamics of the interaction between mucin and NE were assessed by isothermal titration calorimetry (VP-ITC, MicroCal, Northampton, MA). 0.1 g of mucin from porcine stomach (type II) was dissolved in 1 L of PBS (5 mM pH 7.4) to obtain a final concentration of 0.01% w/v and NE were diluted with the same PBS to 0.1% w/v. Both solutions were degassed while stirring for 10 min before the loading. 1.42 mL of the mucin solution were placed into the calorimetric cell equilibrated at 25 °C and titrated by the injection of 283 μ L of NE loaded in the syringe (3 μ L for the first injection, followed by 28 injections of 10 μ L each) under continuous stirring at 307 rpm. The duration of each injection was 20 s, and the time interval between them was 200 s. Control titrations were performed by injecting the same concentration of NE into the reaction cell containing the dilution buffer, using the same injection parameters. The raw data obtained with the control titration were then subtracted to the mucin-nanoemulsion raw data.

2.4.3. 3D-time laps imaging using confocal laser scanning microscopy

The penetration of NE (10% w/v) in artificial gastric mucin type II (10% w/v) was verified by 3D time laps imaging using Confocal Laser Scanning Microscopy (CLSM, Confocal Zeiss LSM 800) available at the Centre Technologique des Microstructures (CT μ) of the University Lyon 1 (Villeurbanne, France).

A constant volume of mucin solution (50 μ L) was filled in a chamber slide resulting in equally thick mucins layers (3 mm). At time zero, 10 μ L of DiD-loaded NE were added on the top of the mucin layer (Fig. S1). Z-stacks (51 images of planes at various depths) within the mucin sample were obtained at a constant distance of 20 μ m from the bottom of the slide. The wavelength for DiD excitation was set at 640 nm and the emission was measured between 646 and 700 nm. Particle penetration was tracked and z-stacks images starting from time 10 min and at time intervals of 10 min up to 3 h were recorded. A sample of mucin alone was examined as control. Images were analysed with the Fiji ImageJ software [38] for fluorescence intensity and 3D visualisation of image stacks.

2.5. Preparation of chitosan sponges and nanoemulsion incorporation process

CH solutions were prepared by dissolving CH in an aqueous solution of acetic acid at 1% w/w under magnetic stirring (375 rpm) for 24 h at room temperature. Mass % of CH reported in Table 1 included

1 ~8% of residual water content. The final CH concentrations were 0.1% w/w (CH A) and 1% w/w (CH
2 B) (Table 1).

3

4 Table 1. Formulated chitosan (CH) and nanoemulsion-loaded chitosan (CH-NE) sponges.

Sample	% (w/w) in CH-NE mixture		% (w/w) in CH-NE sponge		NE/CH ratio (w/w)	Apparent density (g/cm ³)
	CH	NE	CH	NE		
CH A	0.1	–	100	–	–	0.02 ± 0.01
CH B	1	–	100	–	–	0.04 ± 0.01
CH-NE A	0.1	2.5	3.9	96.1	25	0.44 ± 0.03
CH-NE B	1	2.5	28.6	71.4	2.5	0.10 ± 0.05
CH-NE C	1	10	9.1	90.9	10	0.21 ± 0.01

5

6 To prepare CH-NE mixtures, NE were added to CH solutions and the samples were magnetically
7 stirred at 375 rpm for 3 h at room temperature until complete homogenization. CH-NE mixtures at CH
8 concentrations of 0.1% and 1% w/w and NE concentrations of 2.5% and 10% w/w were obtained (CH-
9 NE A, B, C in Table 1). The samples were then transferred to lyophilisation vials to be converted into
10 dry sponges by freeze-casting technique [24]. The freezing and drying steps were carried out in a
11 Cryonext pilot freeze-dryer (Cryonext, Saint-Aunès, France). The freeze-drying process consisted in 3
12 steps: i) freezing at -50 °C for 6 h in the freeze-dryer chamber (cooling speed of 0.3°C·min⁻¹ during the
13 first 3h); ii) primary drying from -50 °C to 0 °C in 20 h (0.1 mbar); iii) secondary drying at 20 °C for 12 h
14 (0.1 mbar for 6h, then 0.01 mbar for other 6h). Finally, the vials were sealed with rubber caps and
15 stored at 20 °C.

16

17 2.6. Microscopy observations of sponges: electron microscopies and optical images

18 Sponge morphology was assessed by scanning electron microscopy (SEM) using a FEI Quanta 250
19 FEG microscope at the Centre Technologique des Microstructures (CTμ) of the University Lyon 1
20 (Villeurbanne, France). Surface and cross-sectional morphology of the sponges were analysed. The
21 samples were coated under vacuum by cathodic sputtering with copper and observed by SEM under
22 an accelerating voltage of 15 kV. Transmission electron microscopy (TEM) was performed with a
23 Philips CM120 microscope at the Centre Technologique des Microstructures (CTμ) of the University
24 Lyon 1 (Villeurbanne, France). Diluted NE (10 μL) was deposited on a microscope grid (copper
25 support coated with carbon) and slowly dried in open air. The dry samples were observed by TEM
26 under 120 kV acceleration voltage. Optical images of sponge surfaces were collected using a Keyence
27 VHX-6000 series digital microscope (Keyence, Jonage, France). Pictures of the depth of pores across
28 a large area of the sponge surface were captured in real-time and combined by 3D image stitching.

29

30 2.7. Rehydration and water uptake capacity

31 The CH and CH-NE sponges were rehydrated at pH 1.2 in simulated gastric fluids (SGF), and at pH 5,
32 5.5 and 7.5 in two different media: PBS (5 mM) and simulated GI fluid in fasted state (FaSSIF-V2).
33 Then, the water uptake capacity was evaluated in PBS and FaSSIF-V2. Pre-weighed freeze-dried
34 sponges (initial mass M_0) were submerged in the media. At predetermined time points, the excess of
35 medium was gently removed using a micropipette, and hydrated sponges were weighed (M_s). The
36 water uptake was calculated as follows:

1 water uptake % = $\frac{M_S - M_0}{M_0} \times 100$ Eq. 2

2

3 **2.8. Rheological characterization**

4 Oscillatory rheological tests were carried out through a MCR 302 rheometer (Anton Paar, Les Ulis,
5 France) fitted with a 25 mm plate-plate geometry. CH and CH-NE sponges were rehydrated in PBS at
6 pH 7.5 for 15 min. The temperature was set at 22 °C. The applied strain ($\gamma\%$) was fixed at 1% within
7 the linear viscoelastic regime on the basis of a previous amplitude sweep test. The apparent storage
8 and loss moduli of rehydrated CH and CH-NE sponges were measured by mean of frequency sweep
9 tests over an angular frequency range of 100–0.05 rad·s⁻¹.

10

11 **2.9. *In vitro* release studies**

12 The *in vitro* release of NE from the CH sponges was evaluated in PBS and FaSSIF-V2 at pH of 5, 5.5
13 and 7.5 by mean of two different studies: destructive and cumulative.

14 The influence of composition and pH of the release medium was assessed by the destructive study.
15 NR-loaded NE were embedded into CH-NE A sponges (52 mg) and 3 mL of release medium were
16 added on the top of sponges. Two different media at three different pH were tested: i) PBS at pH 5, pH
17 5.5, and pH 7.5 ii) FaSSIF-V2 at pH 5, 5.5 and 7.5. At scheduled time points (5 min, 30 min, 2 h, 8 h
18 and 24 h), the release media were retrieved, and the amount of NE released (NR-loaded NE) was
19 measured by UV-vis spectroscopy.

20 Then, the influence of CH and NE concentrations on NE release from the sponges was assessed in
21 FaSSIF-V2 by mean of the cumulative study. To this aim, 5 mL of medium FaSSIF-V2 were added on
22 top of the sponges containing CCM-loaded NE (weight of the dry sponge CH-NE A: 52 mg, B: 70 mg,
23 C: 55 mg and D: 60 mg, at constant CCM concentration of 50 $\mu\text{g}\cdot\text{g}^{-1}$) and the pH was varied over
24 time. FaSSIF-V2 was prepared at pH 7.5 and this pH was maintained for the first 24 h of the study.
25 Then, the pH was decreased to 5.5 for the following 48 h. Finally, the pH value was set at 5 to 72 h.
26 At predetermined time points (30 min, 1, 2, 3, 4, 5, 6, 7, 8, 24, 48, and 72 h), the entire volume of
27 medium was removed and replaced with fresh medium. The amount of CCM released was quantified
28 by HPLC-UV as described above. Data were normalized based on the dry weight of the NE in the
29 sponge.

30

31 **2.10. *In vitro* cell viability studies**

32 **2.10.1 Cell culture conditions**

33 Human colorectal carcinoma (HCT 116) cells were used to perform the MTT assays, being cultured in
34 75 cm² flasks, at 37 °C in a humidified atmosphere 5% CO₂ and 95% air incubator. Cell culture
35 medium was DMEM, supplemented with 10% (v/v) FBS and 1% (v/v) penicillin/streptomycin. The
36 medium was exchanged every two days.

37 Human colon carcinoma (Caco-2) cells were used to perform MTS assays. Caco-2 cells were cultured
38 in 75 cm² flasks, at 37 °C in a humidified atmosphere 5% CO₂ and 95% air incubator. Cell culture
39 medium was DMEM, supplemented with 10% (v/v) FBS, 2% (v/v) penicillin/streptomycin and 1%
40 nanomycopolitine. The medium was exchanged every two days.

41

42 **2.10.2 Toxicological evaluation of NE**

43 The effect of blank NE on the viability of HCT 116 cells was evaluated by the MTT colorimetric assay.
44 To do so, 1x10⁴ cells/well were seeded in 96-well plates and maintained overnight at 37 °C, 5% CO₂.

1 Then, the culture medium was removed, and cells were treated with increasing concentration of blank
2 NE (ranging from 10 to 1250 $\mu\text{g}\cdot\text{mL}^{-1}$) diluted with pre-warmed DMEM supplemented with 2% of FBS
3 (v/v). DMEM was used as positive control (100% viability), while SDS (2% w/v) as negative control.
4 Cells were exposed to the formulations for 3 and 24 h at 37 °C. After the considered period, samples
5 were replaced with 100 μL of fresh medium added of 25 μL of MTT solution (0.5 $\text{mg}\cdot\text{mL}^{-1}$ in PBS pH
6 7.4) in each well. The plates were incubated for 4 h at 37 °C. The formazan purple crystals formed by
7 the reaction of MTT with NAD(P)H of metabolically active cells were dissolved in 100 μL of SDS (10%
8 w/v) and the plates were incubated overnight at 37 °C. The absorbance was measured
9 spectrophotometrically (Infinite M200; Tecan, Austria) at 570 nm, with background correction at
10 650 nm.

11 The effect of blank NE on the viability of Caco-2 cells was evaluated by the MTS assay. To this end,
12 2×10^4 cells/well were seeded in 96-well plates and maintained for 48 h at 37 °C, 5% CO_2 . Then, the
13 culture medium was removed, and cells were treated with increasing concentration of blank NE
14 (ranging from 10 to 1250 $\mu\text{g}\cdot\text{mL}^{-1}$) diluted with pre-warmed DMEM supplemented with 10% of FBS
15 (v/v). DMEM was used as positive control (100% viability), while SDS (3% w/v) as negative control.
16 Cells were exposed to the formulations for 3 and 24 h at 37 °C. After the considered period, samples
17 were replaced with 100 μL of fresh medium added of 20 μL of MTS solution (Promega CellTiter 96™
18 AQueous One Solution Cell Proliferation Assay) in each well. The plates were incubated for 4 h at 37 °C.
19 The absorbance was measured spectrophotometrically (Multiskan EX, Thermo Fisher Scientific,
20 France) at 492 nm, with background correction at 620 nm.

21 Cell viability was calculated by the following formula (Abs = absorbance):

$$22 \text{ Cell viability (\%)} = \frac{\text{Abs sample} - \text{Abs SDS}}{\text{Abs DMEM} - \text{Abs SDS}} \times 100 \quad \text{Eq. 3}$$

23 The IC_{50} were calculated using GraphPad Prism version 8.0.0 for Windows (GraphPad Software, San
24 Diego, California, USA).

25

26 **2.11. *In vivo* biodistribution study of fluorescent NE-loaded sponges following oral** 27 **administration**

28 All animal experiments were approved by the local animal ethics of University Claude Bernard Lyon 1,
29 and carried out in compliance with current French guidelines. Female nude mice (average body weight
30 of 20 g, $n = 45$) used for the experiment were obtained from Charles River Laboratories (Saint-
31 Germain-Nuelles, France). The animals were fasted for 6 h before the oral gavage. Three different
32 systems were administered: i) DiD-loaded NE (NE 10% w/w), ii) DiD-loaded NE mixed with CH
33 solution (CH dissolved in acetic acid), named CH-NE mixture (CH-NE C, CH 1%- NE 10% w/w), and
34 iii) DiD-loaded NE embedded in the CH sponge, defined as CH-NE sponge (CH-NE C, CH 1%- NE
35 10% w/w). NE and CH-NE mixture were administer as liquid colloidal suspensions, while CH-NE
36 sponges were re-hydrated with water and filled in the feeding tube.

37 Mice were randomly divided into three groups: NE ($n = 15$), CH-NE mixture ($n = 15$), CH-NE sponge (n
38 $= 15$). Each formulation contained NE at a concentration of 100 $\text{mg}\cdot\text{mL}^{-1}$, corresponding to a dose of \approx
39 1.25 $\text{mg}\cdot\text{kg}^{-1}$ of body weight.

40 At scheduled time points (1, 2, 3, 4, and 6 h), anesthetized animals were placed prone in a light-tight
41 chamber where a controlled flow of 1.5% isoflurane in air was administered through a nose cone to
42 maintain anaesthesia. Fluorescence images as well as bright-field pictures of mice whole body (ventral
43 view) were acquired via a back-thinned CCD-cooled camera ORCAiBT-512G (Hamamatsu Photonics
44 Deutschland GmbH, Herrsching am Ammersee, Germany) using a coloured glass long-pass RG 665

1 filter (Melles Griot, Voisins les Bretonneaux, France), which cuts off all excitation light. Optical
 2 excitation was carried out at 644 nm, and the emission wavelength was detected at 664 nm. At each
 3 time point (1, 2, 3, 4, and 6 h), n = 3 mice for time point were sacrificed and the organs (GI, liver,
 4 spleen, heart, kidneys, lungs, bone, brain, muscle) were harvested. *Ex vivo* fluorescent measurements
 5 were performed immediately after organ collection to determine the accumulation of the dye. Images
 6 were analysed using the Wasabi software 1.5 (Hamamatsu Photonics Deutschland GmbH, Herrsching
 7 am Ammersee, Germany). The fluorescence intensities of the intestinal segments were normalized
 8 using the min-max normalisation strategy and data mapped to the range 0 to 1 for each mouse. Then,
 9 comparisons between normalized signals were made at all the time points for all different groups.

11 2.12. Statistical analysis

12 The normality of data distribution of the *in vitro* cytotoxicity and *in vivo* studies was assessed by mean
 13 of the Shapiro-Wilk test ($\alpha > 0.05$). *In vitro* cytotoxicity data were analysed by mean of a Student's
 14 t-test to compare different groups. *In vivo* data were analysed by a Two-way ANOVA multiple
 15 comparison (Tukey test). A p-value less than 0.05 indicated statistical significance ($p < 0.05 = *$; $p <$
 16 $0.01 = **$; $p < 0.001 = ***$; $p < 0.0001 = ****$; $\geq 0.05 =$ not significant). Statistical analysis of the data
 17 was performed using GraphPad Prism version 8.0.0 for Windows (GraphPad Software, San Diego,
 18 California, USA). The data are the mean \pm SD for n = 3.

20 3. Results and discussion

21 3.1. Nanoemulsions formulation, physicochemical characterization, and stability

22 Monodisperse lipid nanosystems, namely NE with slightly negative surface charge were designed and
 23 obtained combining emulsion phase inversion (EPI) technique and homogenization process [31]. They
 24 presented a mean droplet size of 104 ± 3 nm, a low Pdl (0.2) and a ζ -potential of -9 ± 1 mV (Table 2).
 25 Due to the presence of the hydrophobic core, Nile red (NR) and curcumin (CCM) dyes were efficiently
 26 loaded, with encapsulation efficiencies around 100%. Moreover, after NR and CCM loading no
 27 alterations in particle hydrodynamic diameter and Pdl were observed, while the ζ -potential was shifted
 28 towards more negative values. The different zeta potential values after loading of dyes might be
 29 attributed to an alteration on the electrical double layer on the nanoparticle surface. The stability of
 30 blank and loaded NE in colloidal suspension (27% w/w, pH 6.8), upon storage at 20 °C, was followed
 31 over 28 days (Fig. S2 in supplementary information). The mean hydrodynamic size and Pdl remained
 32 stable during the examined period. No leakage of the dyes was detected upon 28 days. In a previous
 33 work we showed that the selected NE formulation was stable in both SGF (simulated gastric fluid) and
 34 FaSSIF-V2 fluid (simulated intestinal fluid in fasted state), making them a good system candidate for
 35 oral delivery [31]. Moreover, the NE were successfully converted into dry powders using the freeze-
 36 drying technique enabling their long-term storage [31].

38 Table 2. Physicochemical characteristics of blank and loaded nanoemulsions (NE). NR-NE: Nile red-
 39 loaded NE; CCM-NE: curcumin-loaded NE.

Sample	Size (nm)	Pdl	ζ -potential (mV)	Encapsulation efficiency (%)	
				Day 0	Day 28
Blank NE	104 ± 3	0.2	-9 ± 1	–	–
NR-NE	93 ± 5	0.2	-20 ± 3	99.7 ± 1	100.1 ± 3
CCM-NE	98 ± 8	0.2	-19 ± 5	99.9 ± 4	98.6 ± 5

1

2 **3.2. Mucopenetrating properties of nanoemulsions**

3 To target the intestinal epithelium, delivery systems must diffuse across the mucus layer either to
4 interact with surface receptors of the epithelial cells, or to pass through the epithelium to reach the
5 blood circulation [11]. To predict mucus permeation behaviour, we carried out an in-depth
6 physicochemical characterization of mucin-NE interactions using different techniques: Dynamic Light
7 Scattering (DLS), Isothermal Titration Calorimetry (ITC) and Confocal Laser Scanning Microscopy
8 (CLSM) analysis.

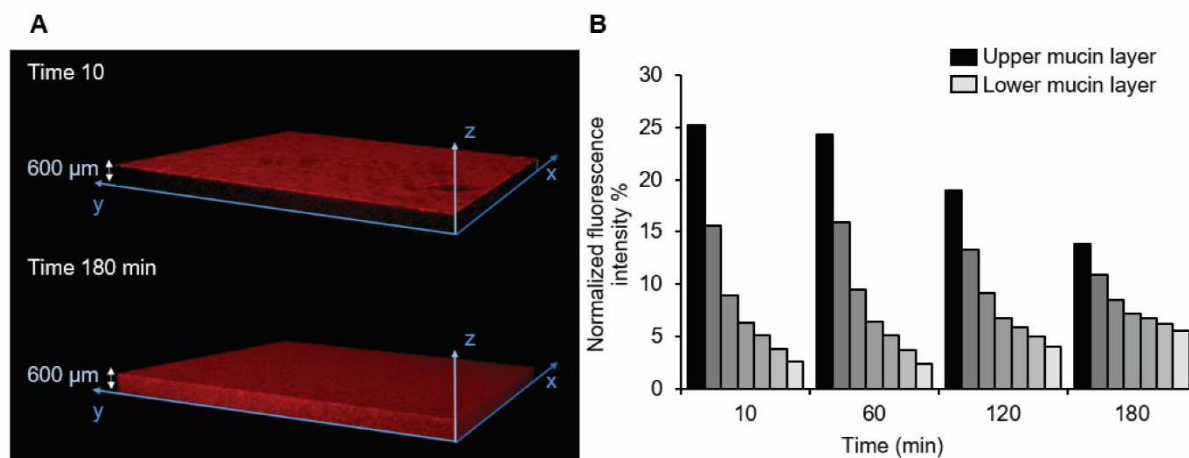
9 As a first approach, we studied the surface ionic interactions of PEGylated NE in presence of
10 reconstituted intestinal mucins by monitoring hydrodynamic diameter and surface charge of the
11 system using DLS over the time. As described by Bernkop-Schnürch group, the contact between
12 negatively charged mucins and nanoparticles can result in a possible adsorption of mucins onto the
13 NE surface through electrostatic interactions, affecting the physicochemical properties of the
14 nanosystem [12]. No increase in particle size (around 100 nm) and no modification of NE ζ -potential
15 (around -8 mV) was observed after incubation of NE (0.5% w/v) with mucins (0.5% w/v) in Sorenson's
16 phosphate buffer (pH 7.4) at 37 °C during 4 h (Fig. S3 A in supplementary information). Due to the
17 neutral surface charge of the NE, the interaction with mucins was avoided.

18 The DLS analysis was further exploited to analyse the behaviour of both mucins and NE at different
19 pH. The mucus at the luminal surface is usually more acidic than the mucin firmly adherent layer near
20 the epithelial interface. Such variation of pH can lead to conformational changes in the mucin structure
21 and induce possible interactions with NE [32]. The ζ -potential of NE (0.1% w/v) and mucin solutions
22 (0.1% w/v) was separately analysed at pH values ranging from 2 to 9 in saline buffer 5 mM at room
23 temperature (Fig. S3 B in supplementary information). Under acidic conditions mucin pH shifted
24 toward neutrality (-0.4 mV) due to the protonation of carboxylic acid residues [39]. The NE followed
25 the same behaviour showing a surface charge close to -0.4 mV. The absence of electrostatic charge
26 and electrostatic repulsions implied that steric forces alone imparted colloidal stabilisation. At neutral
27 pH, both NE and mucins showed a weak negative ζ -potential (around -10 mV). In basic conditions
28 (pH 9), ζ -potential values of about -15 mV were recorded for the two samples. This slightly negative
29 surface charge suggested the presence of repulsive electrostatic forces between nanoparticles and
30 glycosylated proteins and indicated that a polyelectrolyte association will not occur.

31 After establishing that NE and mucins exhibited only weak surface interactions, the thermodynamics of
32 specific interactions between the two systems were studied by calorimetric analysis using ITC [40]. In
33 particular, the nature of the possible non-covalent interactions (electrostatic interactions, van der
34 Waals forces and hydrophobic interactions) was assessed [13]. When NE (0.1% w/v) were titrated
35 over a mucin solution (0.01% w/v) only the presence of low energy peaks was evidenced, a pattern
36 similar to the one obtained during the control titration analysis (Fig. S3 C in supplementary
37 information). We concluded that these low-energy effects were mainly due to the dilution of the NE in
38 the sample cell. In good agreement with the ζ -potential analysis of NE surface properties, this finding
39 suggested the absence of binding affinities between mucins and NE.

40 Along with DLS and ITC experiments, NE displacement in mucins was monitored using 3D-time laps
41 CLSM imaging (Fig. 1). The study was performed in a dedicated chamber slide containing the mucin
42 solution (Fig. S1). At the beginning of the analysis (time point 10 min in Fig. 1 A and B), the majority of
43 NE were located in the upper layer, as demonstrated by the high fluorescent signal. Over the 3 h of
44 analysis, NE diffused to the underneath layers at a speed of $1.3 \mu\text{m}\cdot\text{min}^{-1}$. After 180 min of analysis,

1 fluorescence was observed across the whole mucin sample, meaning that NE distributed in all the
2 sample height (600 μm). (Fig. 1 A and B, video S1 in supplementary information).
3



4
5 Fig. 1. A) Z-stacks of NE penetration (red) in the mucin layer (10% w/v, 600 μm thickness) at time
6 point 10 and 180 min; B) total fluorescence signal of NE in the mucin layer (10% w/v) as a function of
7 time as determined by image analysis software.
8

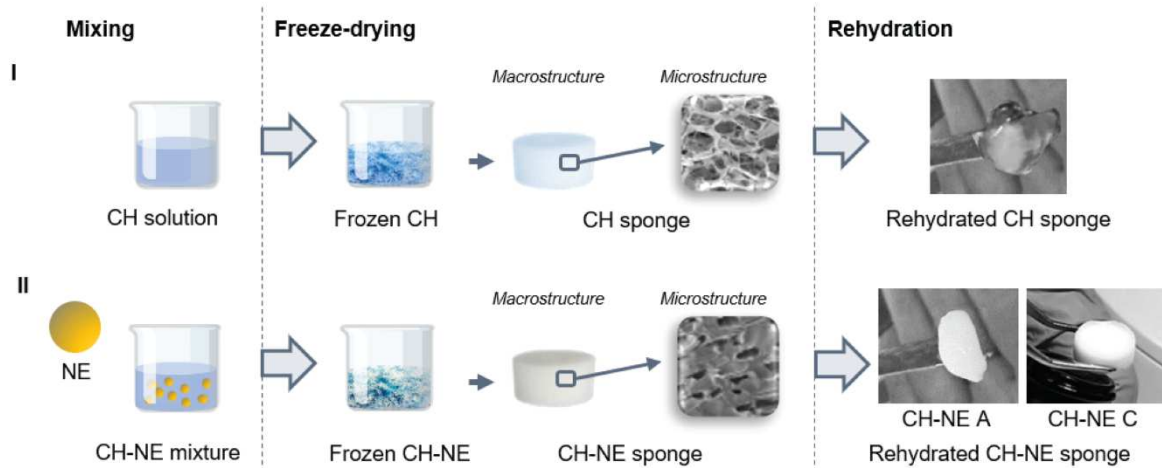
9 Modifications of the nanoparticle surface with hydrophilic polymers, such as polydopamine, dextran-
10 containing polymers or PEG have been described as successful strategies to facilitate mucus
11 penetration [4,11,13,17]. In our study, NE were endowed with penetrating ability by their PEGylated
12 shell (PEG (40) stearate surfactant) which conferred neutral surface properties to NE and reduced
13 association with mucins. By avoiding the entrapment in the mucosal barriers, the developed NE holds
14 promise for reaching the intestinal epithelium and improve drug delivery efficacy.
15

16 3.3. Development of nanoemulsion-loaded chitosan sponges

17 Once assessed the mucopenetrating ability of NE, an original nanocomposite system made of NE
18 loaded in a mucoadhesive CH sponge was designed. CH of low degree of acetylation (DA 4%) and
19 high molecular weight ($M_w 550 \pm 50 \text{ kg}\cdot\text{mol}^{-1}$) was used. High M_w CH has been selected as it provides
20 greater mucoadhesion ability because of the higher molecular interactions with mucins and the
21 increased entanglement of CH molecules in the mucin layer [33].

22 The preparation of CH-NE sponges is illustrated in Fig. 2. Firstly, CH was solubilized in an acetic acid
23 solution (1% w/w). Then, NE were added to CH solution and the CH-NE mixture was stirred to obtain a
24 homogeneous suspension. To produce CH sponges (Fig. 2 I) and nanocomposite sponges (Fig. 2 II),
25 the freeze-casting method was used [24]. By freezing the CH solution or the CH-NE mixture, the solid
26 phase was segregated by the moving freezing front and accumulated between the growing ice
27 crystals, thus determining the structural configuration of the final system. Dry sponges were obtained
28 once ice had been removed by sublimation. The porosity was a replica of the frozen aqueous crystals.
29 The morphology of CH sponges was examined by SEM analysis (Fig. 3).

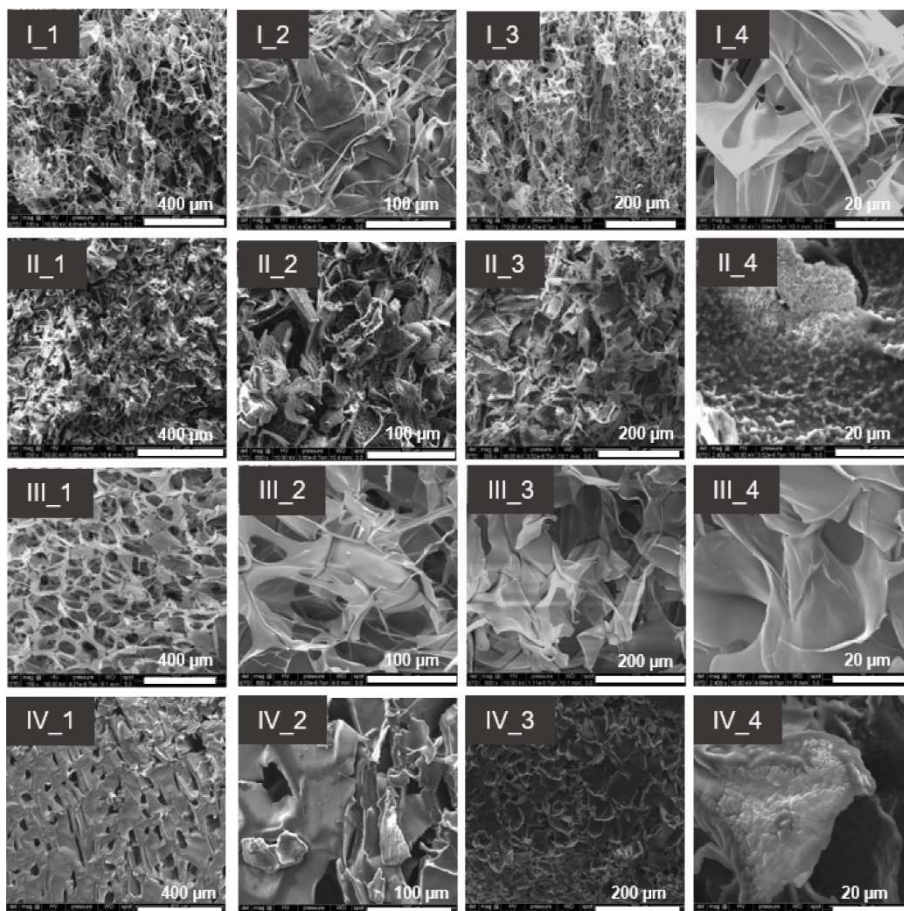
1



2

3 Fig. 2. Formulation process of I) chitosan (CH) sponges and II) nanoemulsion-loaded chitosan (CH-
 4 NE) sponges and their aspect after re-hydration. CH-NE A: sponge at low CH concentration (CH
 5 0.1%- NE 2.5% w/w), CH-NE C: sponge at high CH concentration (CH 1%- NE 10% w/w). CH:
 6 chitosan ($550 \text{ kg} \cdot \text{mol}^{-1}$, DA 4%); NE: nanoemulsion.

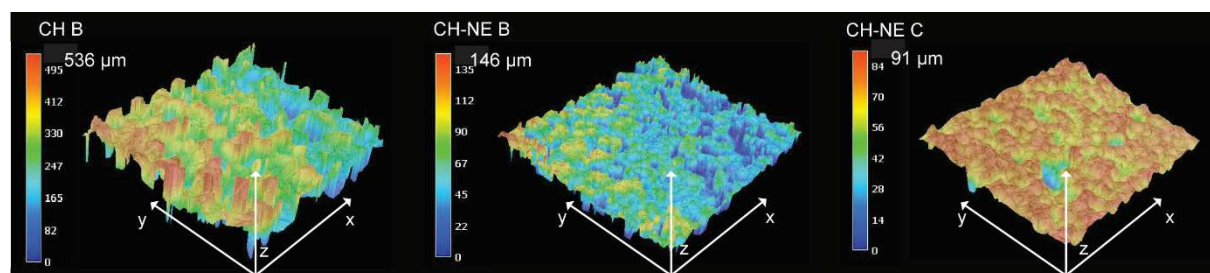
7



8

9 Fig. 3. SEM images of CH and CH-NE sponges. I: CH A; II: CH-NE A; III: CH B; IV: CH-NE C as
 10 defined in table 1. 1: sample surface at low magnification (scale bar: μm); 2: sample surface at higher
 11 magnification (scale bar: $100 \mu\text{m}$); 3: Bulk of the sponge sample at intermediate magnification (scale
 12 bar: $200 \mu\text{m}$); 4 Bulk of the sponge sample at high magnification (scale bar: $20 \mu\text{m}$).

1
2 At low CH concentration (0.1% w/w CH A series I in figure 3), CH sponges were soft and
3 unconsolidated, presenting smooth surfaces. Entangled and non-continuous interpore membranes
4 were present both at the surface and in the bulk of the sponge. As chitosan concentration increased
5 (1% w/w CH B series III in figure 3), consolidated sponges presenting a well-defined cellular structure,
6 interconnected pores and smooth walls were obtained.
7 Upon the loading of NE in CH, sponges presented a different organization characterized by a dense
8 structure and rough surface (Fig. 3 II and 3 IV). Such roughness was ascribed to the accumulation of
9 NE on the sponge surface, as previously reported [41,42]. NE presence in the nanocomposite was
10 also assessed by TEM images (Fig. S4 in supplementary information), showing NE with hydrodynamic
11 size of around 100 nm and spherical shape. At high NE/CH ratio of 25 (CH 0.1% w/w, CH-NE A) the
12 CH interpore membranes were entirely covered in NE because of the excess of NE present (Fig. 3 II).
13 In turn, at NE/CH ratio of 10 (CH 1% w/w, CH-NE C) NE accumulated on CH walls while maintaining
14 the sponge porous structure (Fig. 3 IV). Optical images showed that the depth of the pores at the
15 sponge decreased in presence of NE (535 μm in CH B vs 146 μm in CH-NE B and 90 μm in CH-NE C
16 sponges, Fig. 4). The presence of NE was concomitant with a higher ice nucleation during the freezing
17 process which led to the formation of small crystals and consequently small pores in the sponges [43].
18



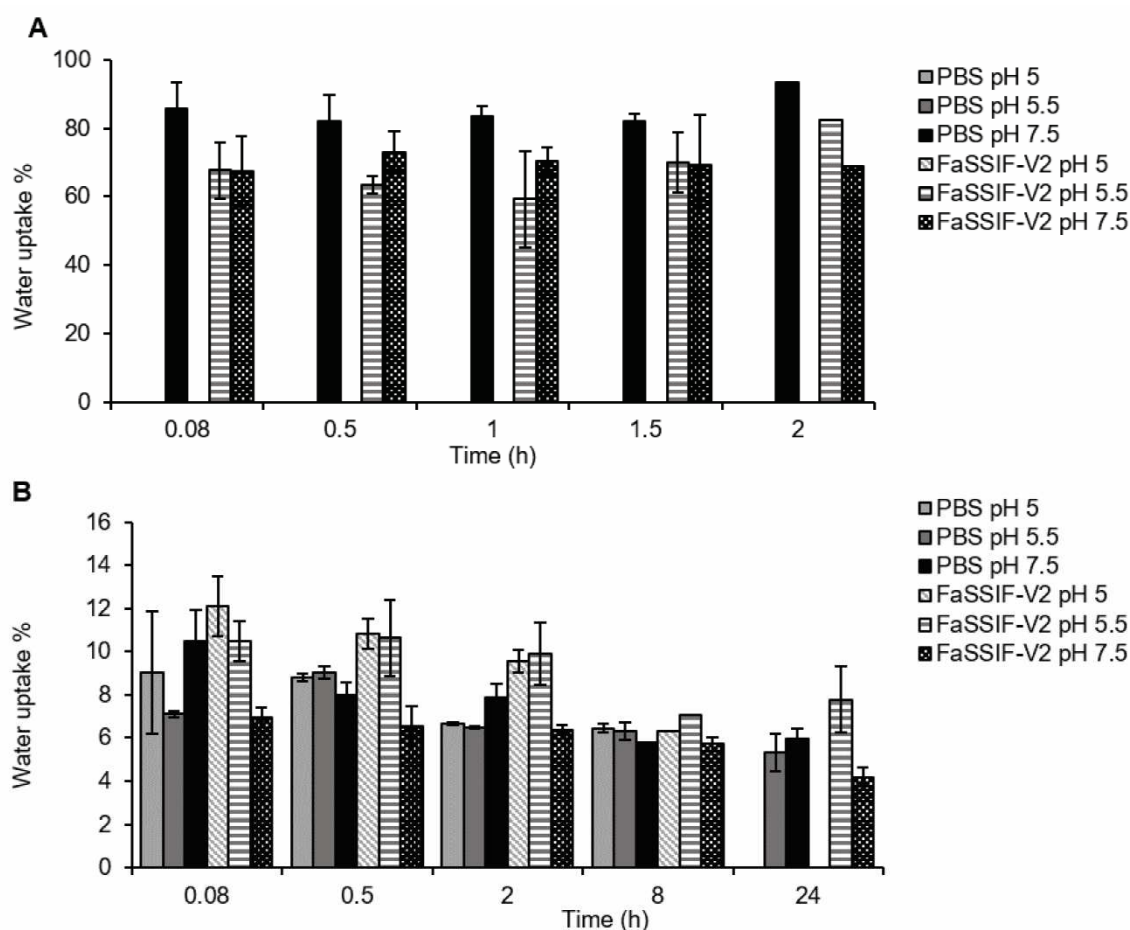
19
20 Fig. 4. Optical images of CH B and CH-NE sponges (CH-NE B and CH-NE C). The z-axis values 535
21 μm , 146 μm and 90 μm represent the maximum depth of the pores on the sponge surface.
22

23 Overall, the amount of CH and NE played a pivotal role in determining the final system morphology
24 and porosity, and the presence of NE conferred stiffness and reinforced the sponge structure.
25

26 3.4. Sponges rehydration: water uptake capacity

27 CH and CH-NE sponges were rehydrated in SGF, PBS and FaSSIF-V2. PBS was used to mimic ion
28 concentration and pH of human body fluids, and SGF and FaSSIF-V2 to mimic the physiological
29 composition of human gastrointestinal fluid [44]. To assess the sponge stability in the acidic
30 environment of the stomach, sponges were firstly evaluated in SGF at pH 1.2 by macroscopic
31 observation of structural changes. The sponges CH-NE A and C were unaffected by the acidic pH and
32 no dissolution occurred within the first 3 h. Then, sponges were studied in PBS and FaSSIF-V2 at pH
33 5, 5.5 and 7.5: such pH range covers the apparent pKa of CH (~6.2) and simulates *in vitro* the human
34 intestinal luminal pH in both healthy (pH of 5.5 in the small bowel and 7.5 in the colon) and
35 inflammatory conditions (reduced pH values mostly in the colon) [3]. Upon rehydration in PBS media,
36 pure CH sponges (0.1% w/w CH A and 1% w/w CH B) dissolved at pH values (pH 5 and 5.5) below
37 the pKa CH (Fig. 5 A). The protonation of amine groups of chitosan allowed its progressive re-
38 dissolution in such acidic aqueous solutions. On the other hand, at pH 5.5 in FaSSIF-V2 medium and
39 at pH of 7.5 in both PBS and FaSSIF-V2, CH sponges (CH A and CH B) turned into hydrogel structure

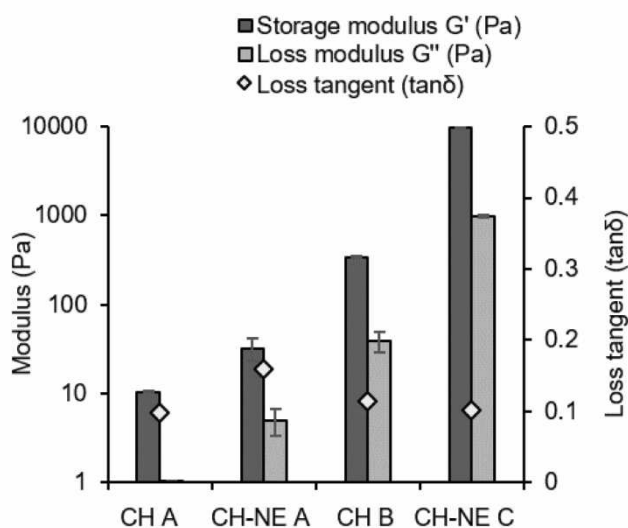
1 able to take-up high water amounts (85% water uptake in PBS at pH 7.5; 70% in FaSSIF-V2 at pH 7.5
 2 and 5.5) (Fig. 5 A and Fig. 2).
 3 A different trend was observed for NE-loaded sponges (Fig. 5 B). When CH-NE sponges prepared at
 4 high NE/CH ratio of 25 (CH 0.1% w/w CH-NE A) were rehydrated, the macrostructure of the dry
 5 sponge collapsed and turned into a dense, aggregated system (Fig. 2). The swelling was immediate,
 6 and no further water uptake occurred over time. Unlike pure CH sponges (0.1% w/w CH A), CH-NE A
 7 did not dissolve at any pH up to 8 h and the complete dissolution only occurred after 24 h at pH 5, in
 8 both PBS and FaSSIF-V2. Instead, at lower CH-NE ratio of 2.5 and 10 (CH 1% w/w CH-NE B and CH-
 9 NE C), the macrostructure of the sponges was not altered upon rehydration (Fig. 2) and all systems
 10 became non pH-responsive, as described in details in session 3.6. The NE loading impaired the ability
 11 of the polymeric structure to retain water: 10% of water, on average, was taken-up by CH-NE sponge
 12 A (Fig. 5 B). This behaviour was related to the high apparent density and low porosity of the
 13 nanocomposite system (table 1) and it could be ascribed to the presence of NE, which enhanced the
 14 hydrophobicity of the systems. In previous studies, the incorporation of a hydrophobic component in
 15 hydrogels was shown to decrease water uptake [45,46]. The slight reduction in water uptake over time
 16 (Fig. 5 B) could be associated with the release of the NE absorbed on the sponge surface in the
 17 rehydration medium, as highlighted in session 3.6.
 18



19 Fig. 5 A) Water uptake capacity of CH A sponge at pH 5, 5.5 and 7.5 in both PBS and FaSSIF-V2; B)
 20 Water uptake capacity of CH-NE A sponge at pH 5, 5.5 and 7.5 in both PBS and FaSSIF-V2.
 21
 22

23 3.5. Rheological analysis

1 The viscoelastic properties of rehydrated sponges were assessed through rheological measurements
 2 in dynamic mode. From amplitude sweep measurements, the linear viscoelastic region was identified
 3 at a shear strain ($\gamma\%$) range of 0.01%–100%, at angular frequency (ω) = 10 rad·s⁻¹ and temperature of
 4 22 °C). Thus, frequency sweep measurements were performed at $\gamma\%$ 1%, ω = 0.05–100 rad·s⁻¹. The
 5 results obtained for sponges with and without NE are given for ω = 1 rad·s⁻¹ in Fig. 6.
 6



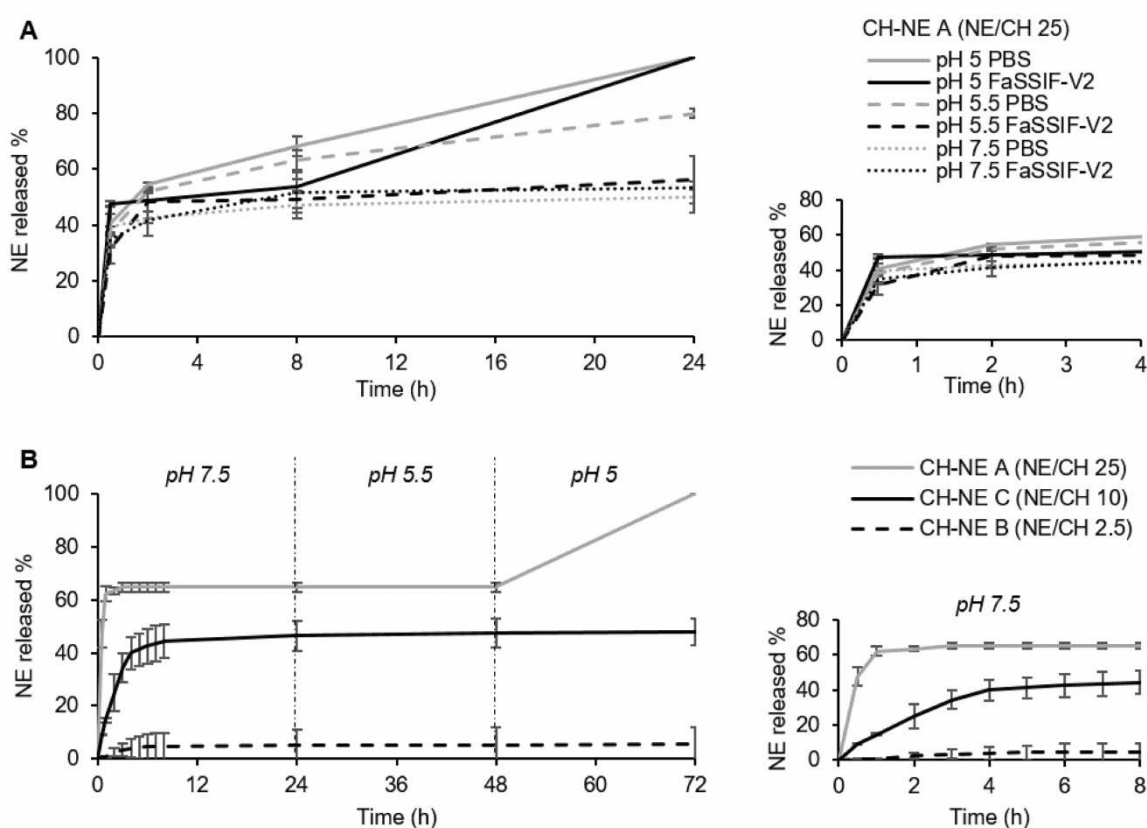
7
 8 Fig. 6. Variation of G' and G'' moduli and loss tangents of rehydrated CH and CH-NE sponges (PBS
 9 pH 7.5) at different CH and NE concentrations at an angular frequency ω = 1 rad·s⁻¹.

10
 11 The frequency sweeps always presented the same trend: the apparent moduli were nearly frequency-
 12 independent, G' was much higher than G'', the loss tangent was always lower than 1 (Table S1),
 13 conditions that define gel-like rheological behaviour. For samples obtained from CH solutions at low
 14 concentration (0.1% w/w CH A and CH-NE A), at high angular frequency (> 10 rad·s⁻¹), the G' and G''
 15 moduli increased with frequency (Fig. S5). This behaviour is typical of that of softer gels [47,48]. The
 16 G' and G'' apparent moduli were higher at higher CH concentration (CH B versus CH A Fig. 7),
 17 indicative of the improved connectivity of the sponge network (see figure 3). Moreover, values of
 18 apparent moduli were higher when CH was loaded with NE, with increasing values at the highest NE
 19 concentrations (10% w/w CH-NE C). In line with previous findings [49,50], the increase in the system
 20 stiffness along with NE addition suggested that NE were able to interact with CH, preventing the
 21 relaxation of CH chains under shear stress. NE also bring hydrophobicity to the sponges and limit
 22 water uptake, thus limiting plasticization effects of chitosan by water. In view of an intestinal delivery,
 23 the mechanical strength of rehydrated sponges is a major asset. A cohesive system, as CH-NE C,
 24 might be suitable to increase the retention time at the intestinal site by avoiding product flow together
 25 with enhancing mucoadhesion.

26
 27 **3.6. *In vitro* release studies**

28 *In vitro* release studies of NE from nanocomposite sponges following rehydration were carried out in
 29 PBS and FaSSIF-V2 at pH 5, 5.5 and 7.5 to investigate i) the role of pH and composition of release
 30 medium (destructive release studies), and ii) the influence of the sponge composition (NE/CH ratio) on
 31 the nanosystem release kinetics (cumulative release studies). **The aim of the release studies was to**

1 evaluate the behavior of the nanosystem *per se*. Therefore, all release studies were carried out under
 2 non-sink conditions to avoid the premature release of the hydrophobic dye loaded in the NE core.
 3 Fig. 7 A shows how pH and composition of the release medium affected NE release (destructive
 4 release studies). The study was performed on samples at NE/CH ratio of 25 (CH-NE A). When
 5 sponges were incubated with PBS at pH 5 and 5.5, 65% of NE were released within 8 h. In the case of
 6 PBS at pH 7.5, only 47% of NE were released over the same experimental period.
 7 Such release behaviour at pH values lower than the pKa of CH (6.2) can be related to the protonation
 8 of CH amino groups, resulting in the increase of CH solubility, which weakens the structure of the
 9 sponge. In the release study performed in FaSSIF-V2 at pH 5, 5.5 and 7.5, 50% of NE were released
 10 over 8 h of incubation irrespective of the medium pH. After 24 h, CH sponges completely dissolved
 11 and 100% of NE were released at pH 5 in both PBS and FaSSIF-V2. Lower release rates were
 12 observed at the two other pH: 80% release at pH 5.5 in PBS, 50% release at pH 5.5 and pH 7.5 in
 13 FaSSIF-V2. These results highlighted the impact of the release medium composition on the NE
 14 release profile. FaSSIF-V2 contains amphiphilic molecules, such as sodium taurocholate (NaTC) and
 15 lecithin, able to interact with the nanocomposites, thus increasing the hydrophobicity of the sponge
 16 and slowing down the release rate. Lecithin can have affinity for the hydrophobic regions formed by
 17 the hydrophobic interactions NE-CH and NE-NE [51,52]. Diversely, NaTC binds strongly to the
 18 nanocomposite thanks to hydrophobic and electrostatic interactions between the negatively charged
 19 sulfonate groups of the surfactant and the amino groups of CH, which are partly protonated at pH 5
 20 and 5.5, forming insoluble micelle-like clusters [40].
 21



22
 23 Fig. 7. A) NE release (Nile Red-loaded NE (NR-NE), 20 $\mu\text{g}\cdot\text{mL}^{-1}$) from the nanocomposite sponge CH-
 24 NE A in PBS and FaSSIF-V2 at pH 5, 5.5 and 7.5 up to 24 h; destructive release study to evaluate the
 25 effect of pH and release medium; B) NE release (curcumin-loaded NE (CCM-NE), CCM 50 $\mu\text{g}\cdot\text{mL}^{-1}$)

1 from nanocomposite sponges at different NE and CH concentrations in FaSSIF-V2 at pH 7.5 up to
2 24 h, pH 5.5 up to 48 h and pH 5 up to 72 h; cumulative release study to evaluate the effect of
3 chitosan and nanoemulsions concentration.

4
5 The physicochemical properties of NE released from the rehydrated nanocomposites were also
6 investigated (in PBS at pH 7.5). NE showed a slight increase in the hydrodynamic diameter ($128 \pm$
7 3 nm vs $104 \pm 3 \text{ nm}$), while ζ -potential values shifted from -9 mV to -2 mV , indicative of the
8 absorption of some chitosan chains on the particle surface.

9 A cumulative release study was performed to investigate the influence of the sponge composition
10 expressed as NE/CH ratio on the release kinetic of NE. Release studies were performed in FaSSIF-V2
11 and the pH was decreased from 7.5 to 5 over 72 h (Fig. 7 B). The sponge at high NE/CH ratio of 25
12 (CH-NE A) fastly released 47% of NE in 30 min, reaching 65% after 3 h. When the NE/CH ratio was
13 decreased to 10 (CH-NE C) the release became sustained. The 9% of NE was released in 30 min,
14 34% in 3 h and a plateau at 46% was reached at 8 h. The further decrease in the NE/CH ratio at 2.5
15 (CH-NE B) prevented the NE release. After 24 h, the pH was lowered at 5.5 and no changes in the
16 release profile were observed up to 48 h. Thus, at time point 48 h, the pH was further decreased until
17 5. The sponge at NE/CH ratio of 25 (CH-NE A) dissolved in one day and 100% of NE was released.
18 Instead, in the sponges at NE/CH ratio of 2.5 and 10 (CH-NE B and C) the release rate remained
19 constant (plateau at 65% release for CH-NE D and at 50% for CH-NE C). These observations were in
20 agreement with the morphological evaluation and suggested that part of the NE was on the bulk of the
21 membranes constituting the pores of the sponges, while part of the NE was located at the sponge
22 surface (see figure 3). NE can interact with the CH polymer chains via hydrogen bonding and
23 hydrophobic interactions, thanks to CH hydrophobicity (4% DA in the neutralized state) [52,53]. In the
24 sponge at NE/CH ratio of 25, NE was present in excess at the surface and the sponge lost its porous
25 nature, as highlighted by the SEM images (Fig. 3 series II). This excess of NE was easily and rapidly
26 released from the sponge surface once in contact with the medium. Then, the remaining NE was
27 constantly released by diffusion through the sponge creating a plateau. Instead, at a NE/CH ratio of 10,
28 a lower amount of NE accumulated on the surface, in fact the sponge maintained its porous structure
29 (SEM images Fig. 3 series IV and optical images Fig. 4). The main mechanism of NE release was the
30 diffusion of the NE present in the bulk of the pore walls. The hydrogen bonds and hydrophobic
31 interactions between CH and NE together with the interconnected 3D network of the sponge
32 microstructure supported the NE diffusion and led to a controlled and prolonged release over time.
33 Similarly, Kassem et al. described a sustained release of the hydrophilic drug buspirone hydrochloride
34 from chitosan sponges by increasing the polymer concentration from 0.5% to 2% thus decreasing the
35 ratio between drug and polymer [23].

36 The absence of release in CH-NE B sponge was not due to the disruption of the nanoparticle, but
37 suggested that when the NE/CH ratio was low (NE/CH 2.5) all the NE were entrapped in the sponge
38 structure, supposedly strongly interacting with the CH polymer chains. Complete NE release of 100%
39 was achieved only in the sponge at high NE/CH ratio of 25 (CH-NE A) when the pH was shifted
40 towards acidic value of 5 due to the sponge dissolution and massive release of particles from the
41 surface of the sponge walls. Possible reasons of the CH-NE A sponge dissolution are i) the lower CH
42 concentration in the initial suspension that led to lower thickness of the interpore membranes and to a
43 higher amount of NE in the bulk of pore membranes, and ii) the modification of the crystalline structure
44 of CH in presence of NE. Further evaluation of the nanocomposite crystallinity will assist in gaining a

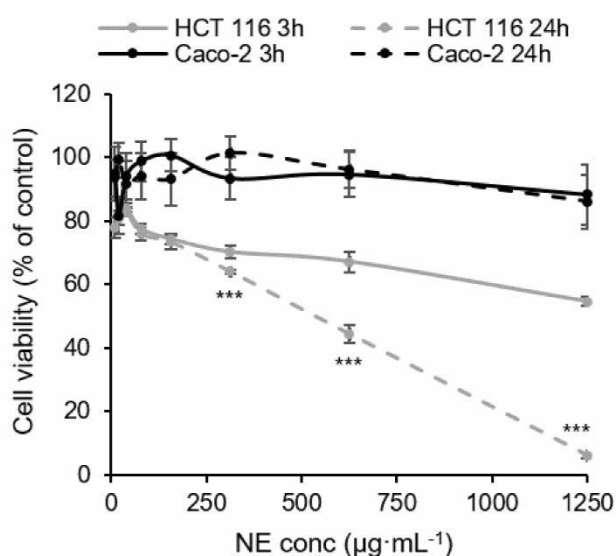
1 better understanding of the NE release kinetics. Thus, in sponges CH-NE B and C, 100% of release
 2 could be achieved only after degradation in the colon by bacterial enzymes and human chitinases [2].
 3 Overall, these results showed that by varying the NE/CH ratio we were able to modulate the release
 4 rate of NE. Several strategies have been reported in the literature to tune the release of nanosystems
 5 from their composite systems as i) the modulation of the degree of cross-linking in polymeric hydrogels
 6 [54,55], ii) the *in situ* hydrogelation of polymers followed by their selective pH triggered degradation
 7 [18], iii) the chemically driven erosion of the nanocomposite hydrogel network at the site of action [56].
 8 In this work a sustained release was obtained by loading NE in CH sponges at NE/CH ratio of 10 (CH-
 9 NE C). Compared to previously designed CH-based materials [57], these CH sponges offer the
 10 advantages of protecting NE from the harsh environment of the GI tract and of tackling shortcomings
 11 related to the CH pH-dependent strength, such as the rapid dissolution and the immediate release of
 12 the associated nanosystem.

13

14 3.7. *In vitro* cytotoxicity

15 Cell viability assays were carried out to evaluate the cytocompatibility of blank NE on two separate
 16 intestinal cell lines, the HCT 116 and the Caco-2. Human colon carcinoma Caco-2 cells are commonly
 17 used as a model of intestinal barrier since upon differentiation they express a phenotype comparable
 18 to enterocytes [58]. Human colorectal carcinoma HCT 116 cells are considered a model of colon
 19 cancer primary cells [59].

20 The *in vitro* cell viability assay was conducted by exposing both cell lines to NE for 3 and 24 h in
 21 concentrations ranging from 10 to 1250 $\mu\text{g}\cdot\text{mL}^{-1}$ (Fig. 8). The minimum level acceptable of cell viability
 22 in cytotoxicity tests was fixed at 70% according to ISO 10993 [60].



23

24 Fig. 8. Cell viability of HCT-116 and Caco-2 cells after exposure to blank NE for 3 h and 24 h.
 25 Statistical data analysis: $p < 0.05 = *$; $p < 0.01 = **$; $p < 0.001 = ***$; $\geq 0.05 =$ not significant.

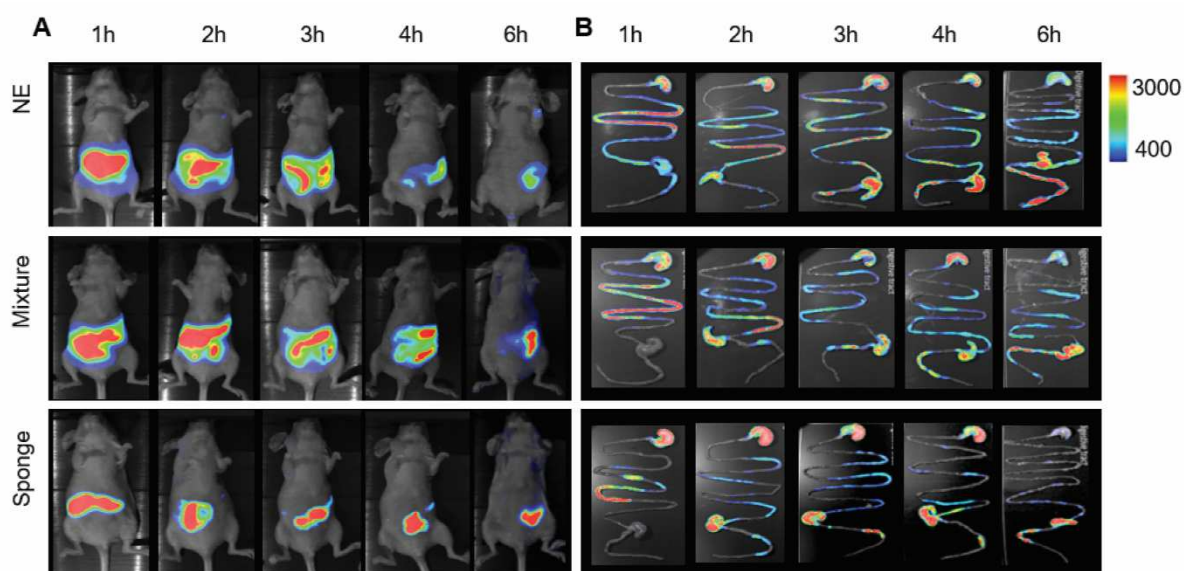
26

27 After the first 3 h, for the HCT 116 cells, blank NE did not show signs of cytotoxicity with a cell viability
 28 above 80% up to 625 $\mu\text{g}\cdot\text{mL}^{-1}$, while it reduced cell viability at the highest concentration used (1250
 29 $\mu\text{g}\cdot\text{mL}^{-1}$, $p=0.01$). After 24 h blank NE showed toxicity at concentration higher than 156 $\mu\text{g}\cdot\text{mL}^{-1}$, being
 30 the IC50 value of 336 $\mu\text{g}\cdot\text{mL}^{-1}$. The value of IC50 of the blank NE was similar to that previously
 31 reported for lipid nanocapsules [59], polymeric nanocapsules [61,62] and solid lipid nanoparticles [63]
 32 when evaluated on the same colon cancer cell line (HCT-116).

1 Regarding to the Caco-2 cell line, their viability remained higher than 80% even at higher NE
 2 concentrations ($1250 \mu\text{g}\cdot\text{mL}^{-1}$) for both time points tested, in accordance with other studies [15,64].
 3 The difference in cytotoxicity between the two cell lines can be ascribed to the different % of FBS
 4 used. In the case of HCT 116 cells a 2% of FBS was required to ensure cell growth. While in the case
 5 of Caco-2 cells 10% FBS was used.
 6 Overall results showed that the cytocompatibility of the NE here developed was in an acceptable
 7 range and opened the way to its future use as delivery system for systemic or localized treatment.
 8 Since the cell viability might be altered by the shielding effect of the CH sponge, future studies will
 9 investigate the toxicity profile of the developed nanocomposite.

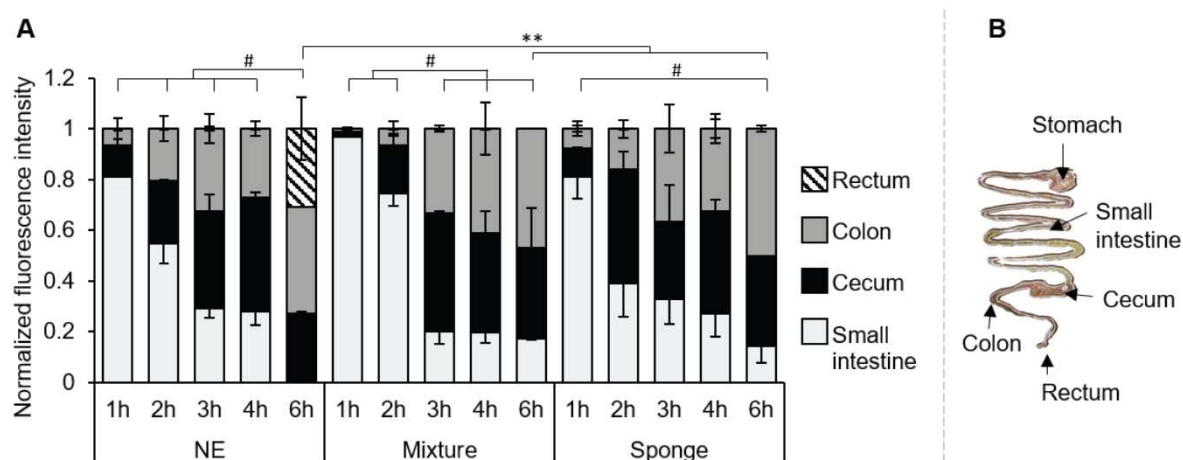
11 3.8. *In vivo* biodistribution and transit studies in mice

12 A variety of methods has been reported in the literature for assessing GI transit times, motility, and
 13 drug release. *In vivo* biodistribution studies using fluorescent or radio-labelled nanoparticles have
 14 been largely used to localize the nanosystems in the GI tract [62]. In this work, we evaluated the
 15 residence time of fluorescent DiD-labelled CH-NE mixture (before freeze-drying) and CH-NE sponges
 16 in the GI tract by near-infrared fluorescence imaging following oral administration to healthy mice. DiD-
 17 loaded NE were also used as control. Observations were made at 1, 2, 3, 4, and 6 h to anesthetized
 18 mice. Due to the short duration of the anaesthesia and the rapid recovery time, the effect of
 19 anaesthesia on GI motility was not expected. Time points were chosen according to previous studies
 20 considering that mice have a total GI transit time of about 6 h and that the majority of the intestinal
 21 content is located in small intestines and cecum after 3 h [65]. The *in vivo* biodistribution profiles of
 22 formulations following oral administration are shown in Fig. 9 A. A wide distribution of the fluorescent
 23 signal in the mice GI region was observed for all the systems. After 6 h, the fluorescent signal still was
 24 detected in the mice GI tract and it was more intense for CH-NE mixture and CH-NE sponge than for
 25 the NE.
 26



27 Fig. 9. A) Fluorescent images of mice whole body; B) representative *ex vivo* fluorescence images of
 28 intestines of mice sacrificed at 1, 2, 3, 4 and 6 h after oral administration of nanoemulsions (NE), CH-
 29 NE mixture (Mixture), CH-NE sponge (Sponge).
 30
 31

1 To perform a semi-quantitative analysis of the fluorescent dye distribution, organs were harvested and
 2 *ex vivo* images were taken (Fig. 9 B). The images collected at the different time points were processed
 3 to extract different information on residence time, targeting ability and potential toxic effect of the
 4 formulations. 1 h after oral gavage, NE had transited through the stomach labelling almost the entire
 5 loop of small intestines and the cecum. At 3 h, NE were visualized mainly in the cecum, ascending,
 6 transverse and descending tract of the colon, and the rectum. After 6 h, only a weak fluorescent signal
 7 was still present in the small intestine while the most intense fluorescence was found in the rectum
 8 (Fig. 9 B and 10 A).
 9 A different transit time was observed when the NE were mixed with the CH solution (CH-NE mixture).
 10 After 2 h and 3 h, an intense fluorescence signal was located in the cecum. NE were retained up to
 11 4 h in cecum and colon and no fluorescent signal was detected in the rectum up to 6 h (Fig. 9 B and
 12 10 A).
 13 On the other hand, when the CH-NE sponge was administered the intestinal residence time was
 14 considerably enhanced. The highest level of fluorescent signal was detected in the cecum up to 6 h
 15 (Fig. 9 B and 10 A). Such behaviour was ascribed to the CH mucoadhesive ability. However, the
 16 fluorescence signal coming from NE embedded in the sponge was less intense as compared to those
 17 obtained with the NE or CH-NE mixture. This observation suggested that the DiD fluorescence was
 18 quenched and that the NE fluorescence intensity was underestimated in the composite formulation.
 19 Quenching typically occurs when lipophilic fluorescent labels are tightly packed together in the
 20 nanoparticle core, as previously observed for other nanocarriers [66], and it can be further enhanced
 21 by the shield effects of the macro-system [29].
 22



23 **Fig. 10. A)** Contents of nanoemulsion (NE), NE-loaded chitosan mixture (Mixture), NE-loaded chitosan
 24 sponge (Sponge) in different parts of the intestinal tract following oral administration at time 1, 2, 3, 4
 25 and 6 h. Statistical data analysis: Significant difference between samples (NE or Mixture or Sponge): p
 26 $< 0.05 = *$; $p < 0.01 = **$; $p < 0.001 = ***$; $p < 0.0001 = ****$; $p \geq 0.05 =$ not significant; Significant
 27 difference from time points within one sample (NE or Mixture or Sponge): $p < 0.05 = \#$, details on the
 28 level of significance can be found in table S2; **B)** Dissection scheme of the mouse GI tract.

30
 31 We also verified by visual inspection the absence of alteration of the intestinal mucosa indicating
 32 absence of toxicity, and preservation of the physiology and gastrointestinal integrity. Moreover, using
 33 *In Vivo* Imaging System (IVIS) technique NE fluorescent signal was not observed in kidneys, liver,
 34 spleen, heart, brain, muscles, lungs, bones, skin and urine. These data suggest that the developed

1 nanocomposite can be investigated for prolonging the intestinal residence time of associated drugs
2 thus allowing for their sustained systemic absorption or enhanced local therapeutic efficacy in the case
3 of inflammatory intestinal pathologies. Similar approaches have been previously reported for
4 nanoparticle-loaded hydrogels. Laroui et al. formulated a cross-linked chitosan and alginate hydrogel
5 to encapsulate nanoparticles containing the anti-inflammatory tripeptide Lys-Pro-Val (KPV) that
6 reduced mucosal inflammation *in vivo* [18]. Nanoparticles containing CD98 siRNA or plasmid DNA
7 embedded in hydrogel were also used target small and large intestine [2,3]. Finally, nanocomposite
8 made of alginate loaded nanoparticles has been described for improving the systemic absorption of
9 oral insulin [20].

10 In this study, the intestinal sustained release and prolonged residence deriving from the synergy
11 between NE mucopenetrating and CH mucoadhesive properties can bring additional therapeutic
12 benefits. **Moreover, the nanocomposite can be tailored to allocate hydrophilic or hydrophobic drugs.**
13 **The system filling in enteric capsules prior to oral administration is envisaged for high effectiveness at**
14 **the intestinal site *in vivo*.**

16 **4. Conclusions**

17 Nanocomposites combining mucopenetrating NE and mucoadhesive CH sponges aimed to prolong
18 intestinal drug delivery by oral administration were successfully designed. PEGylated NE were
19 selected due to their mucopenetrating properties and successfully embedded in CH sponges via the
20 freeze-casting technique without alteration of their physicochemical properties. The combination of
21 different CH and NE concentrations allowed to tune the sponge structural and mechanical properties
22 and to modulate the NE release. The NE cytocompatibility on both Caco-2 and HCT 116 intestinal cell
23 models was demonstrated *in vitro*. Lastly, the nanocomposite oral administration to mice proved the
24 effectiveness in increasing the intestinal residence time. The unique technological and biological
25 properties of this system will be uncovered for the local or systemic improvement in drug therapeutic
26 efficacy.

28 **Acknowledgements:**

29 The research leading to these results has received funding from National Research Agency (ANR),
30 HyDNano project (ANR-18-CE18-0025-01), the PHC Pessoa Programme between ANR and
31 Fundação para a Ciência e Tecnologia (FCT): NanoSpeed, (N° 42306YB) and from FCT project
32 UID/Multi/04326/2019.

34 **Compliance with ethical standards**

35 **Conflict of interest** The authors declare that they have no known competing financial interests or
36 personal relationships that could have appeared to influence the work reported in this paper.

37 **Animal studies** All animal experiments were approved by the local animal ethics of University Claude
38 Bernard Lyon 1 and carried out in compliance with current French guidelines.

40 **References**

- 41 [1] X. Liu, C. Steiger, S. Lin, G.A. Parada, J. Liu, H.F. Chan, H. Yuk, N. V. Phan, J. Collins, S.
42 Tamang, G. Traverso, X. Zhao, Ingestible hydrogel device, Nat. Commun. 10 (2019) 493.
43 doi:10.1038/s41467-019-08355-2.
44 [2] M.D. Bhavsar, M.M. Amiji, Gastrointestinal distribution and *in vivo* gene transfection studies
45 with nanoparticles-in-microsphere oral system (NiMOS), J. Control. Release. 119 (2007) 339–
46 348. doi:10.1016/j.jconrel.2007.03.006.

- 1 [3] H. Laroui, D. Geem, B. Xiao, E. Viennois, P. Rakhya, T. Denning, D. Merlin, Targeting
2 Intestinal Inflammation With CD98 siRNA/PEI-loaded Nanoparticles, *Mol. Ther.* 22 (2014) 69–
3 80. doi:10.1038/mt.2013.214.
- 4 [4] Y. Song, Y. Shi, L. Zhang, H. Hu, C. Zhang, M. Yin, L. Chu, X. Yan, M. Zhao, X. Zhang, H. Mu,
5 K. Sun, Synthesis of CSK-DEX-PLGA Nanoparticles for the Oral Delivery of Exenatide to
6 Improve Its Mucus Penetration and Intestinal Absorption, *Mol. Pharm.* 16 (2019) 518–532.
7 doi:10.1021/acs.molpharmaceut.8b00809.
- 8 [5] E. Taipaleenmäki, B. Städler, Recent Advancements in Using Polymers for Intestinal
9 Mucoadhesion and Mucopenetration, *Macromol. Biosci.* 20 (2020) 1900342.
10 doi:10.1002/mabi.201900342.
- 11 [6] V. Andretto, A. Rosso, S. Briançon, G. Lollo, Nanocomposite systems for precise oral delivery
12 of drugs and biologics, *Drug Deliv. Transl. Res.* (2021). [https://doi.org/10.1007/s13346-021-](https://doi.org/10.1007/s13346-021-00905-w)
13 [00905-w](https://doi.org/10.1007/s13346-021-00905-w).
- 14 [7] S.F. Pantze, J. Parmentier, G. Hofhaus, G. Fricker, Matrix liposomes: A solid liposomal
15 formulation for oral administration, *Eur. J. Lipid Sci. Technol.* 116 (2014) 1145–1154.
16 doi:10.1002/ejlt.201300409.
- 17 [8] B. Menchicchi, J.P. Fuenzalida, K.B. Bobbili, A. Hensel, M.J. Swamy, F.M. Goycoolea,
18 Structure of Chitosan determines its interactions with mucin, *Biomacromolecules.* 15 (2014)
19 3550–3558. doi:10.1021/bm5007954.
- 20 [9] S. Kootala, L. Filho, V. Srivastava, V. Linderberg, A. Moussa, L. David, S. Trombotto, T.
21 Crouzier, Reinforcing Mucus Barrier Properties with Low Molar Mass Chitosans,
22 *Biomacromolecules.* 19 (2018) 872–882. doi:10.1021/acs.biomac.7b01670.
- 23 [10] W. Niebel, K. Walkenbach, A. Béduneau, Y. Pellequer, A. Lamprecht, Nanoparticle-based
24 clodronate delivery mitigates murine experimental colitis, *J. Control. Release.* 160 (2012) 659–
25 665. doi:10.1016/j.jconrel.2012.03.004.
- 26 [11] B. Poinard, S. Kamaluddin, A.Q.Q. Tan, K.G. Neoh, J.C.Y. Kah, Polydopamine Coating
27 Enhances Mucopenetration and Cell Uptake of Nanoparticles, *ACS Appl. Mater. Interfaces.* 11
28 (2019) 4777–4789. doi:10.1021/acsami.8b18107.
- 29 [12] I. Pereira de Sousa, C. Steiner, M. Schmutzler, M.D. Wilcox, G.J. Veldhuis, J.P. Pearson, C.W.
30 Huck, W. Salvenmoser, A. Bernkop-Schnürch, Mucus permeating carriers: formulation and
31 characterization of highly densely charged nanoparticles, *Eur. J. Pharm. Biopharm.* 97 (2015)
32 273–279. doi:10.1016/j.ejpb.2014.12.024.
- 33 [13] Q. Xu, L.M. Ensign, N.J. Boylan, A. Schön, X. Gong, J.-C. Yang, N.W. Lamb, S. Cai, T. Yu, E.
34 Freire, J. Hanes, Impact of Surface Polyethylene Glycol (PEG) Density on Biodegradable
35 Nanoparticle Transport in Mucus ex Vivo and Distribution in Vivo, *ACS Nano.* 9 (2015) 9217–
36 9227. doi:10.1021/acs.nano.5b03876.
- 37 [14] R. Nunes, F. Araújo, J. Tavares, B. Sarmento, J. das Neves, Surface modification with
38 polyethylene glycol enhances colorectal distribution and retention of nanoparticles, *Eur. J.*
39 *Pharm. Biopharm.* 130 (2018) 200–206. doi:10.1016/j.ejpb.2018.06.029.
- 40 [15] A. Jaradat, M.H. Macedo, F. Sousa, K. Arkill, C. Alexander, J. Aylott, B. Sarmento, Prediction
41 of the enhanced insulin absorption across a triple co-cultured intestinal model using mucus
42 penetrating PLGA nanoparticles, *Int. J. Pharm.* 585 (2020) 119516.
43 doi:10.1016/j.ijpharm.2020.119516.
- 44 [16] S. Peers, P. Alcouffe, A. Montembault, C. Ladavière, Embedment of liposomes into chitosan
45 physical hydrogel for the delayed release of antibiotics or anaesthetics, and its first ESEM
46 characterization, *Carbohydr. Polym.* 229 (2020) 115532. doi:10.1016/j.carbpol.2019.115532.
- 47 [17] E. Taipaleenmäki, G. Christensen, E. Brodzkij, S.A. Mouritzen, N. Gal, S. Madsen, M.S.
48 Hedemann, T.A. Knudsen, H.M. Jensen, S.L. Christiansen, F.V. Sparsø, B. Städler,
49 Mucopenetrating polymer – Lipid hybrid nanovesicles as subunits in alginate beads as an oral
50 formulation, *J. Control. Release.* 322 (2020) 470–485. doi:10.1016/j.jconrel.2020.03.047.
- 51 [18] H. Laroui, G. Dalmaso, H.T.T. Nguyen, Y. Yan, S. V. Sitaraman, D. Merlin, Drug-Loaded
52 Nanoparticles Targeted to the Colon With Polysaccharide Hydrogel Reduce Colitis in a Mouse
53 Model, *Gastroenterology.* 138 (2010) 843–853. doi:10.1053/j.gastro.2009.11.003.
- 54 [19] M. Moaddab, J. Nourmohammadi, A.H. Rezayan, Bioactive composite scaffolds of
55 carboxymethyl chitosan-silk fibroin containing chitosan nanoparticles for sustained release of
56 ascorbic acid, *Eur. Polym. J.* 103 (2018) 40–50. doi:10.1016/j.eurpolymj.2018.03.032.
- 57 [20] M. Alfatama, L.Y. Lim, T.W. Wong, Alginate–C18 Conjugate Nanoparticles Loaded in
58 Tripolyphosphate-Cross-Linked Chitosan–Oleic Acid Conjugate-Coated Calcium Alginate
59 Beads as Oral Insulin Carrier, *Mol. Pharm.* 15 (2018) 3369–3382.
60 doi:10.1021/acs.molpharmaceut.8b00391.

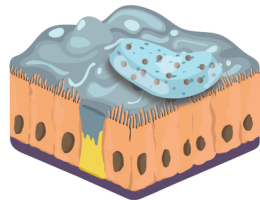
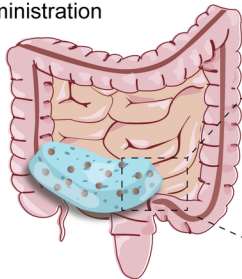
- 1 [21] M. Wang, Y. Ma, Y. Sun, S.Y. Hong, S.K. Lee, B. Yoon, L. Chen, L. Ci, J.-D. Nam, X. Chen, J.
2 Suhr, Hierarchical Porous Chitosan Sponges as Robust and Recyclable Adsorbents for Anionic
3 Dye Adsorption, *Sci. Rep.* 7 (2017) 18054. doi:10.1038/s41598-017-18302-0.
- 4 [22] H.A. Hazzah, R.M. Farid, M.M.A. Nasra, M.A. EL-Massik, O.Y. Abdallah, Lyophilized sponges
5 loaded with curcumin solid lipid nanoparticles for buccal delivery: Development and
6 characterization, *Int. J. Pharm.* 492 (2015) 248–257. doi:10.1016/j.ijpharm.2015.06.022.
- 7 [23] M.A.A. Kassem, A.N. ElMeshad, A.R. Fares, Lyophilized Sustained Release Mucoadhesive
8 Chitosan Sponges for Buccal Bupirone Hydrochloride Delivery: Formulation and In Vitro
9 Evaluation, *AAPS PharmSciTech.* 16 (2015) 537–547. doi:10.1208/s12249-014-0243-3.
- 10 [24] T. De Witte, A.M. Wagner, L.E. Fratila-Apachitei, A.A. Zadpoor, N.A. Peppas, Immobilization of
11 nanocarriers within a porous chitosan scaffold for the sustained delivery of growth factors in
12 bone tissue engineering applications, *J. Biomed. Mater. Res. Part A.* 108 (2020) 1122–1135.
13 doi:10.1002/jbm.a.36887.
- 14 [25] R.C. Feitosa, D.C. Geraldés, V.L. Beraldo-de-Araújo, J.S.R. Costa, L. Oliveira-Nascimento,
15 Pharmacokinetic Aspects of Nanoparticle-in-Matrix Drug Delivery Systems for Oral/Buccal
16 Delivery, *Front. Pharmacol.* 10 (2019) 1057. doi:10.3389/fphar.2019.01057.
- 17 [26] A. Martín-Illana, F. Notario-Pérez, R. Cazorla-Luna, R. Ruiz-Caro, M.D. Veiga, Smart Freeze-
18 Dried Bigels for the Prevention of the Sexual Transmission of HIV by Accelerating the Vaginal
19 Release of Tenofovir during Intercourse, *Pharmaceutics.* 11 (2019) 232.
20 doi:10.3390/pharmaceutics11050232.
- 21 [27] T. Kim, J.U. Kim, K. Yang, K. Nam, D. Choe, E. Kim, I.-H. Hong, M. Song, H. Lee, J. Park, Y.H.
22 Roh, Nanoparticle-Patterned Multicompartmental Chitosan Capsules for Oral Delivery of
23 Oligonucleotides, *ACS Biomater. Sci. Eng.* 4 (2018) 4163–4173.
24 doi:10.1021/acsbiomaterials.8b00806.
- 25 [28] Q. Zhu, J. Talton, G. Zhang, T. Cunningham, Z. Wang, R.C. Waters, J. Kirk, B. Eppler, D.M.
26 Klinman, Y. Sui, S. Gagnon, I.M. Belyakov, R.J. Mumper, J.A. Berzofsky, Large intestine-
27 targeted, nanoparticle-releasing oral vaccine to control genitorectal viral infection, *Nat. Med.* 18
28 (2012) 1291–1296. doi:10.1038/nm.2866.
- 29 [29] L. Hou, Y. Shi, G. Jiang, W. Liu, H. Han, Q. Feng, J. Ren, Y. Yuan, Y. Wang, J. Shi, Z. Zhang,
30 Smart nanocomposite hydrogels based on azo crosslinked graphene oxide for oral colon-
31 specific drug delivery, *Nanotechnology.* 27 (2016) 315105. doi:10.1088/0957-
32 4484/27/31/315105.
- 33 [30] M.N. Corstens, C.C. Berton-Carabin, P.T. Elichiry-Ortiz, K. Hol, F.J. Troost, A.A.M. Masclee, K.
34 Schroën, Emulsion-alginate beads designed to control in vitro intestinal lipolysis: Towards
35 appetite control, *J. Funct. Foods.* 34 (2017) 319–328. doi:10.1016/j.jff.2017.05.003.
- 36 [31] A. Rosso, G. Lollo, Y. Chevalier, N. Troung, C. Bordes, S. Bourgeois, O. Maniti, T. Granjon, P.-
37 Y. Dugas, S. Urbaniak, S. Briançon, Development and structural characterization of a novel
38 nanoemulsion for oral drug delivery, *Colloids Surfaces A Physicochem. Eng. Asp.* 593 (2020)
39 124614. doi:10.1016/j.colsurfa.2020.124614.
- 40 [32] B. Menchicchi, J.P. Fuenzalida, A. Hensel, M.J. Swamy, L. David, C. Rochas, F.M. Goycoolea,
41 Biophysical Analysis of the Molecular Interactions between Polysaccharides and Mucin,
42 *Biomacromolecules.* 16 (2015) 924–935. doi:10.1021/bm501832y.
- 43 [33] A. Mendes, J. Sevilla Moreno, M. Hanif, T. E.L. Douglas, M. Chen, I. Chronakis, Morphological,
44 Mechanical and Mucoadhesive Properties of Electrospun Chitosan/Phospholipid Hybrid
45 Nanofibers, *Int. J. Mol. Sci.* 19 (2018) 2266. doi:10.3390/ijms19082266.
- 46 [34] A. Hirai, H. Odani, A. Nakajima, Determination of degree of deacetylation of chitosan by ¹H
47 NMR spectroscopy, *Polym. Bull.* 26 (1991) 87–94. doi:10.1007/BF00299352.
- 48 [35] A. Montebault, C. Viton, A. Domard, Physico-chemical studies of the gelation of chitosan in a
49 hydroalcoholic medium, 26 (2005) 933–943. doi:10.1016/j.biomaterials.2004.03.033.
- 50 [36] Y. Liu, M. Siard, A. Adams, M.L. Keowen, T.K. Miller, F. Garza, Jr., F.M. Andrews, N.P.
51 Seeram, Simultaneous quantification of free curcuminoids and their metabolites in equine
52 plasma by LC-ESI-MS/MS, *J. Pharm. Biomed. Anal.* 154 (2018) 31–39.
53 doi:10.1016/j.jpba.2018.03.014.
- 54 [37] G. Lollo, G. Ullio-Gamboa, E. Fuentes, K. Matha, N. Lautram, J.-P. Benoit, In vitro anti-cancer
55 activity and pharmacokinetic evaluation of curcumin-loaded lipid nanocapsules, *Mater. Sci.*
56 *Eng. C.* 91 (2018) 859–867. doi:10.1016/j.msec.2018.06.014.
- 57 [38] J. Schindelin, I. Arganda-Carreras, E. Frise, V. Kaynig, M. Longair, T. Pietzsch, S. Preibisch, C.
58 Rueden, S. Saalfeld, B. Schmid, J.-Y. Tinevez, D.J. White, V. Hartenstein, K. Eliceiri, P.
59 Tomancak, A. Cardona, Fiji: an open-source platform for biological-image analysis, *Nat.*
60 *Methods.* 9 (2012) 676–682. doi:https://doi.org/10.1016/j.jconrel.2017.12.034.

- 1 [39] G. Ramírez-García, L. Trapiella-Alfonso, F. D'Orlyé, A. Varenne, Electrophoretic Methods for
2 Characterizing Nanoparticles and Evaluating Their Bio-interactions for Their Further Use as
3 Diagnostic, Imaging, or Therapeutic Tools, in: *Capill. Electromigr. Sep. Methods*, Elsevier,
4 2018: pp. 397–421. doi:10.1016/B978-0-12-809375-7.00019-8.
- 5 [40] M. Thongngam, D.J. McClements, Isothermal titration calorimetry study of the interactions
6 between chitosan and a bile salt (sodium taurocholate), *Food Hydrocoll.* 19 (2005) 813–819.
7 doi:10.1016/j.foodhyd.2004.11.001.
- 8 [41] T. Furst, G.R. Dakwar, E. Zagato, A. Lechanteur, K. Remaut, B. Evrard, K. Braeckmans, G.
9 Piel, Freeze-dried mucoadhesive polymeric system containing pegylated lipoplexes: Towards a
10 vaginal sustained released system for siRNA, *J. Control. Release.* 236 (2016) 68–78.
11 doi:10.1016/j.jconrel.2016.06.028.
- 12 [42] R. Ikono, N. Li, N.H. Pratama, A. Vibriani, D.R. Yuniarni, M. Luthfansyah, B.M. Bachtiar, E.W.
13 Bachtiar, K. Mulia, M. Nasikin, H. Kagami, X. Li, E. Mardiyati, N.T. Rochman, T. Nagamura-
14 Inoue, A. Tojo, Enhanced bone regeneration capability of chitosan sponge coated with TiO₂
15 nanoparticles, *Biotechnol. Reports.* 24 (2019). doi:10.1016/j.btre.2019.e00350.
- 16 [43] S. Deville, Freeze-casting of porous biomaterials: Structure, properties and opportunities,
17 *Materials (Basel).* 3 (2010) 1913–1927. doi:10.3390/ma3031913.
- 18 [44] D.M. Mudie, N. Samiei, D.J. Marshall, G.E. Amidon, C.A.S. Bergström, Selection of In Vivo
19 Predictive Dissolution Media Using Drug Substance and Physiological Properties, *AAPS J.* 22
20 (2020) 34. doi:10.1208/s12248-020-0417-8.
- 21 [45] M. Dai, X. Zheng, X. Xu, X. Kong, X. Li, G. Guo, F. Luo, X. Zhao, Y.Q. Wei, Z. Qian, Chitosan-
22 Alginate Sponge: Preparation and Application in Curcumin Delivery for Dermal Wound Healing
23 in Rat, *J. Biomed. Biotechnol.* 2009 (2009) 1–8. doi:10.1155/2009/595126.
- 24 [46] C.A. Schoener, H.N. Hutson, N.A. Peppas, pH-responsive hydrogels with dispersed
25 hydrophobic nanoparticles for the delivery of hydrophobic therapeutic agents, *Polym. Int.* 61
26 (2012) 874–879. doi:10.1002/pi.4219.
- 27 [47] K. Almdal, J. Dyre, S. Hvidt, O. Kramer, Towards a phenomenological definition of the term
28 'gel', *Polym. Gels Networks.* 1 (1993) 5–17. doi:10.1016/0966-7822(93)90020-I.
- 29 [48] A. Montebault, C. Viton, A. Domard, Rheometric study of the gelation of chitosan in a
30 hydroalcoholic medium, *Biomaterials.* 26 (2005) 1633–1643.
31 doi:10.1016/j.biomaterials.2004.06.029.
- 32 [49] H. Liu, K. Nakagawa, D. Chaudhary, Y. Asakuma, M.O. Tadé, Freeze-dried macroporous foam
33 prepared from chitosan/xanthan gum/montmorillonite nanocomposites, *Chem. Eng. Res. Des.*
34 89 (2011) 2356–2364. doi:10.1016/j.cherd.2011.02.023.
- 35 [50] A.D. Woolfson, M.L. Umrethia, V.L. Kett, R.K. Malcolm, Freeze-dried, mucoadhesive system
36 for vaginal delivery of the HIV microbicide, dapivirine: Optimisation by an artificial neural
37 network, *Int. J. Pharm.* 388 (2010) 136–143. doi:10.1016/j.ijpharm.2009.12.042.
- 38 [51] P. Knoos, A. V. Svensson, S. Ulvenlund, M. Wahlgren, Release of a poorly soluble drug from
39 hydrophobically modified poly (acrylic acid) in simulated intestinal fluids, *PLoS One.* 10 (2015)
40 1–16. doi:10.1371/journal.pone.0140709.
- 41 [52] J. Becerra, G. Sudre, I. Royaud, R. Montserret, B. Verrier, C. Rochas, T. Delair, L. David,
42 Tuning the Hydrophilic/Hydrophobic Balance to Control the Structure of Chitosan Films and
43 Their Protein Release Behavior, *AAPS PharmSciTech.* 18 (2017) 1070–1083.
44 doi:10.1208/s12249-016-0678-9.
- 45 [53] M. Goldberg, A. Manzi, E. Aydin, G. Singh, P. Khoshkenar, A. Birdi, B. LaPorte, A. Krauskopf,
46 G. Powell, J. Chen, R. Langer, Development of a Nanoparticle-Embedded Chitosan Sponge for
47 Topical and Local Administration of Chemotherapeutic Agents, *J. Nanotechnol. Eng. Med.* 5
48 (2014) 040905. doi:10.1115/1.4030899.
- 49 [54] W. Gao, D. Vecchio, J. Li, J. Zhu, Q. Zhang, V. Fu, J. Li, S. Thamphiwatana, D. Lu, L. Zhang,
50 Hydrogel Containing Nanoparticle-Stabilized Liposomes for Topical Antimicrobial Delivery,
51 *ACS Nano.* 8 (2014) 2900–2907. doi:10.1021/nn500110a.
- 52 [55] L. Racine, A. Guliyeva, I. Wang, V. Larreta-Garde, R. Auzély-Velty, I. Texier, Time-Controllable
53 Lipophilic-Drug Release System Designed by Loading Lipid Nanoparticles into Polysaccharide
54 Hydrogels, *Macromol. Biosci.* 17 (2017) 1700045. doi:10.1002/mabi.201700045.
- 55 [56] W. Zhu, Y. Li, L. Liu, Y. Chen, C. Wang, F. Xi, Supramolecular Hydrogels from Cisplatin-
56 Loaded Block Copolymer Nanoparticles and α -Cyclodextrins with a Stepwise Delivery Property,
57 *Biomacromolecules.* 11 (2010) 3086–3092. doi:10.1021/bm100889j.
- 58 [57] A. Worthen, K. Irving, Y. Lapitsky, Supramolecular Strategy Effects on Chitosan Bead Stability
59 in Acidic Media: A Comparative Study, *Gels.* 5 (2019) 11. doi:10.3390/gels5010011.
- 60 [58] Y. Sambuy, I. De Angelis, G. Ranaldi, M.L. Scarino, A. Stamatii, F. Zucco, The Caco-2 cell

- 1 line as a model of the intestinal barrier: influence of cell and culture-related factors on Caco-2
2 cell functional characteristics, *Cell Biol. Toxicol.* 21 (2005) 1–26. doi:10.1007/s10565-005-
3 0085-6.
- 4 [59] G. Lollo, K. Matha, M. Bocchiardo, J. Bejaud, I. Marigo, A. Virgone-Carlotta, T. Dehoux, C.
5 Rivière, J.-P. Rieu, S. Briçon, T. Perrier, O. Meyer, J.-P. Benoit, Drug delivery to tumours
6 using a novel 5-FU derivative encapsulated into lipid nanocapsules, *J. Drug Target.* 27 (2019)
7 634–645. doi:10.1080/1061186X.2018.1547733.
- 8 [60] International Organization for Standardization, ISO 10993-1 Biological Evaluation of Medical
9 Devices—Part, Vol. 5, Tests for in Vitro Cytotoxicity, Geneva Switz. (2009).
- 10 [61] I. Štaka, A. Cadete, B.T. Surikutchi, H. Abuzaid, T.D. Bradshaw, M.J. Alonso, M. Marlow, A
11 novel low molecular weight nanocomposite hydrogel formulation for intra-tumoural delivery of
12 anti-cancer drugs, *Int. J. Pharm.* 565 (2019) 151–161. doi:10.1016/j.ijpharm.2019.04.070.
- 13 [62] G. Lollo, A. Gonzalez-Paredes, M. Garcia-Fuentes, P. Calvo, D. Torres, M.J. Alonso,
14 Polyarginine Nanocapsules as a Potential Oral Peptide Delivery Carrier, *J. Pharm. Sci.* 106
15 (2017) 611–618. doi:10.1016/j.xphs.2016.09.029.
- 16 [63] L. Ferreira, Carneiro, Silva, Pacheco, Souza-Fagundes, Goes, Oliveira, Correa, Formation of
17 ion pairing as an alternative to improve encapsulation and anticancer activity of all-trans
18 retinoic acid loaded in solid lipid nanoparticles, *Int. J. Nanomedicine.* 7 (2012) 6011–6020.
19 doi:10.2147/IJN.S38953.
- 20 [64] T.J. Wooster, S.C. Moore, W. Chen, H. Andrews, R. Addepalli, R.B. Seymour, S.A. Osborne,
21 Biological fate of food nanoemulsions and the nutrients they carry – internalisation, transport
22 and cytotoxicity of edible nanoemulsions in Caco-2 intestinal cells, *RSC Adv.* 7 (2017) 40053–
23 40066. doi:10.1039/C7RA07804H.
- 24 [65] P. Padmanabhan, J. Grosse, A.B.M.A. Asad, G.K. Radda, X. Golay, Gastrointestinal transit
25 measurements in mice with 99mTc-DTPA-labeled activated charcoal using NanoSPECT-CT,
26 *EJNMMI Res.* 3 (2013) 60. doi:10.1186/2191-219X-3-60.
- 27 [66] H. Zhang, S.C. De Smedt, K. Remaut, Fluorescence Correlation Spectroscopy to find the
28 critical balance between extracellular association and intracellular dissociation of mRNA
29 complexes, *Acta Biomater.* 75 (2018) 358–370. doi:10.1016/j.actbio.2018.05.016.
- 30

Nanoemulsions-Chitosan NANOCOMPOSITE SPONGES

Oral administration



Enhanced intestinal residence time

Chitosan mucoadhesion
Nanoemulsion mucopenetration



Nanocomposite



Mucus layer



Enterocyte



Goblet cell